Accurate first-derivative nonadiabatic couplings for the H_3 system

Ravinder Abrol,[a] Amy Shaw, and Aron Kuppermann[b]
Arthur Amos Noyes Laboratory of Chemical Physics, Division of Chemistry and Chemical Engineering, California Institute of Technology, Pasadena, California 91125

David R. Yarkony
Department of Chemistry, The Johns Hopkins University, Baltimore, Maryland 21218

(Received 11 May 2001; accepted 19 June 2001)

A conical intersection exists between the ground ($1\,^2A'$) and the first-excited ($2\,^2A'$) electronic potential energy surfaces (PESs) of the H_3 system for C_{3v} geometries. This intersection induces a geometric phase effect, an important factor in accurate quantum mechanical reactive scattering calculations, which at low energies can be performed using the ground PES only, together with appropriate nuclear motion boundary conditions. At higher energies, however, such calculations require the inclusion of both the $1\,^2A'$ and $2\,^2A'$ electronic PESs and the corresponding nuclear derivative couplings. Here we present *ab initio* first-derivative couplings for these states obtained by analytic gradient techniques and a fit to these results. We also present a fit to the corresponding $1\,^2A'$ and $2\,^2A'$ adiabatic electronic PESs, obtained from the *ab initio* electronic energies. The first-derivative couplings are compared with their approximate analytical counterparts obtained by Varandas *et al.* [J. Chem. Phys. **86**, 6258 (1987)] using the double many-body expansion method. As expected, the latter are accurate close to conical intersection configurations but not elsewhere. We also present the contour integrals of the *ab initio* couplings along closed loops around the above-mentioned conical intersection, which contain information about possible interactions between the $2\,^2A'$ and $3\,^2A'$ states. © *2001 American Institute of Physics.*
[DOI: 10.1063/1.1390510]

I. INTRODUCTION

The quantum theory of chemical reaction dynamics on the ground adiabatic electronic potential energy surface (PES) has developed appreciably over the years. It has been applied successfully to study the dynamics of reactions involving three atoms[1–3] and is being applied to reactions involving four[4,5] or more atoms.

For any polyatomic system involving three or more atoms, the ground and the first-excited adiabatic electronic PESs can intersect even if the corresponding states have the same symmetry and spin multiplicity.[6] These intersections, which are usually conical, occur quite frequently in polyatomic systems. The reason is that these polyatomic systems possess three or more internal nuclear motion degrees of freedom, and only two independent relations between three electronic Hamiltonian matrix elements are sufficient for the existence of doubly degenerate electronic energy eigenvalues. As a result, these relations between those matrix elements are easily satisfied and explain the frequent occurrence of conical intersections. Assuming the adiabatic electronic wave functions to be real and as continuous as possible in the nuclear coordinate space, if the polyatomic system is transported around a closed loop in that space (a so-called pseudorotation) that encircles a conical intersection geometry, these electronic wave functions must change sign.[6,7] This change of sign has consequences for the structure and dynamics of the polyatomic system, as it requires the corresponding nuclear wave functions to undergo a compensatory change of sign, known as the geometric phase (GP) effect,[8–12] to keep the total wave function single valued. This sign change is a special case of Berry's geometric phase,[11] and is also referred to as the molecular Aharonov–Bohm effect.[13] It greatly affects the nature of the solutions of the corresponding nuclear motion Schrödinger equation.[12,14] Accurate quantum mechanical reactive scattering calculations (on the ground electronic PES), with and without the GP effect included, have been carried out for the $H+H_2$ system and its isotopic variants ($D+H_2$ and $H+D_2$)[14–18] to obtain differential and integral cross sections. The cross sections obtained with the GP effect included were in much better agreement with the experimental results[19–22] than those obtained with the GP effect excluded. Hence, the GP effect is an important factor in accurate quantum scattering calculations done on the ground adiabatic electronic PES.

A review of the one- and two-electronic state Born–Huang[23,24] (also usually called Born–Oppenheimer) approximations has been given in detail elsewhere[12] and only the features pertinent to this paper are briefly summarized here. In the one-electronic-state approximation, the GP effect has to be imposed on the adiabatic nuclear wave functions in order to obtain accurate results at low energies. At energies above the conical intersection energy, when this approximation breaks down, the effect of the first-excited electronic PES has to be included explicitly in the scattering calcula-

[a]Work done in partial fulfillment of requirements for Ph.D. in Chemistry.
[b]Author to whom correspondence should be addressed; electronic mail: aron@caltech.edu

tions to obtain accurate results. In the adiabatic representation, the GP effect still has to be imposed on each of the two state nuclear wave functions. In this two-electronic-state approximation,[12] the nuclear motion Schrödinger equation for an N-atom system is

$$\left[-\frac{\hbar^2}{2\mu}\{\nabla_{\mathbf{R}}^2\mathbf{I}+2\mathbf{W}^{(1)\mathrm{ad}}(\mathbf{q})\cdot\nabla_{\mathbf{R}}+\mathbf{W}^{(2)\mathrm{ad}}(\mathbf{q})\}+\{\boldsymbol{\epsilon}^{\mathrm{ad}}(\mathbf{q})-E\mathbf{I}\}\right]\boldsymbol{\chi}^{\mathrm{ad}}(\mathbf{R})=\mathbf{0}, \tag{1}$$

where $\mathbf{R}$ is a set of $3(N-1)$ nuclear coordinates (remaining after the removal of the center of mass coordinates), and $\mathbf{q}$ is a set of $3(N-2)$ internal nuclear coordinates obtained by removing from the set $\mathbf{R}$ three Euler angles which orient a nuclear body-fixed frame with respect to a space-fixed one. As an example, for a triatomic system $\mathbf{R}$ can be a set of principal axes of inertia body-fixed symmetrized hyperspherical coordinates $(\rho,\theta,\phi_\lambda,a_\lambda,b_\lambda,c_\lambda)$,[12,14] and $\mathbf{q}$ is then comprised of ρ, θ, and ϕ_λ since the remaining $a_\lambda,b_\lambda,c_\lambda$, are Euler angles. In addition, $\mathbf{I}$ is a 2×2 identity matrix,

$$\boldsymbol{\chi}^{\mathrm{ad}}(\mathbf{R})=\begin{pmatrix}\chi_1^{\mathrm{ad}}(\mathbf{R})\\ \chi_2^{\mathrm{ad}}(\mathbf{R})\end{pmatrix} \tag{2}$$

is a 2×1 column vector whose elements are the ground $[\chi_1^{\mathrm{ad}}(\mathbf{R})]$ and the first-excited $[\chi_2^{\mathrm{ad}}(\mathbf{R})]$ adiabatic nuclear motion wave functions, and

$$\boldsymbol{\epsilon}^{\mathrm{ad}}(\mathbf{q})=\begin{pmatrix}\epsilon_1^{\mathrm{ad}}(\mathbf{q}) & 0\\ 0 & \epsilon_2^{\mathrm{ad}}(\mathbf{q})\end{pmatrix} \tag{3}$$

is a diagonal matrix whose diagonal elements are the ground $[\epsilon_1^{\mathrm{ad}}(\mathbf{q})]$ and the first-excited $[\epsilon_2^{\mathrm{ad}}(\mathbf{q})]$ adiabatic electronic PESs.

$\mathbf{W}^{(1)\mathrm{ad}}(\mathbf{q})$ and $\mathbf{W}^{(2)\mathrm{ad}}(\mathbf{q})$ are respectively, the first-derivative[25–28] and second-derivative[25,29,30] nonadiabatic coupling matrix elements between the ground and first-excited adiabatic electronic PESs. For the two-electronic-state approximation they are 2×2 matrices, whose elements are defined by

$$\mathbf{W}_{m,n}^{(1)\mathrm{ad}}(\mathbf{q})=\langle\psi_m^{\mathrm{ad}}(\mathbf{r};\mathbf{q})|\nabla_{\mathbf{R}}\psi_n^{\mathrm{ad}}(\mathbf{r};\mathbf{q})\rangle_{\mathbf{r}}, \tag{4}$$

$$W_{m,n}^{(2)\mathrm{ad}}(\mathbf{q})=\langle\psi_m^{\mathrm{ad}}(\mathbf{r};\mathbf{q})|\nabla_{\mathbf{R}}^2\psi_n^{\mathrm{ad}}(\mathbf{r};\mathbf{q})\rangle_{\mathbf{r}}, \tag{5}$$

where $\mathbf{r}$ is a set of electronic coordinates, and m and n refer to the ground or the first-excited electronic PESs. $\psi_n^{\mathrm{ad}}(\mathbf{r};\mathbf{q})$ is an eigenfunction of the electronic Hamiltonian and satisfies the electronic Schrödinger equation

$$[\hat{H}^{\mathrm{el}}-\epsilon_n^{\mathrm{ad}}(\mathbf{q})]\psi_n^{\mathrm{ad}}(\mathbf{r};\mathbf{q})=0. \tag{6}$$

$\psi_n^{\mathrm{ad}}(\mathbf{r};\mathbf{q})$ and $\epsilon_n^{\mathrm{ad}}(\mathbf{q})$ depend only on the internal nuclear coordinates $\mathbf{q}$ because the Coulombic interaction potential between the (N-atom) system's particles (nuclei and electrons), which appears in $\hat{H}^{\mathrm{el}}$, depends only on their relative distances and hence these quantities depend on $\mathbf{q}$ but not on the three Euler angles which orient the nuclear frame with respect to a space-fixed one. This introduces small rotational coupling terms that are two orders of magnitude or more smaller than the remaining coupling terms and can be neglected. This leads to a subtle but important point implicit in Eqs. (4) and (5): although the right-hand sides of these equations contain $\mathbf{R}$, the left-hand sides contain only $\mathbf{q}$. Also, since $\nabla_{\mathbf{R}}$ and $\nabla_{\mathbf{R}}^2$ are, respectively, the gradient and Laplacian operators, $\mathbf{W}_{m,n}^{(1)\mathrm{ad}}(\mathbf{q})$ is a vector quantity and $W_{m,n}^{(2)\mathrm{ad}}(\mathbf{q})$ is a scalar quantity.

The matrix $\mathbf{W}^{(1)\mathrm{ad}}(\mathbf{q})$ is skew Hermitian, and if we choose $\psi_1^{\mathrm{ad}}(\mathbf{r};\mathbf{q})$ and $\psi_2^{\mathrm{ad}}(\mathbf{r};\mathbf{q})$ to be real, it is skew symmetric and $\mathbf{W}_{1,1}^{(1)\mathrm{ad}}(\mathbf{q})$ and $\mathbf{W}_{2,2}^{(1)\mathrm{ad}}(\mathbf{q})$ are identically zero. Furthermore, the off-diagonal elements, $\mathbf{W}_{1,2}^{(1)\mathrm{ad}}(\mathbf{q})$ and $\mathbf{W}_{2,1}^{(1)\mathrm{ad}}(\mathbf{q})$, satisfy the relation

$$\mathbf{W}_{1,2}^{(1)\mathrm{ad}}(\mathbf{q})=-\mathbf{W}_{2,1}^{(1)\mathrm{ad}}(\mathbf{q}). \tag{7}$$

The presence of the first-derivative term $\mathbf{W}^{(1)\mathrm{ad}}(\mathbf{q})\cdot\nabla_{\mathbf{R}}$ in Eq. (1) introduces inefficiencies in the numerical solution of this equation. A diabatic representation[12,31] of this equation is introduced to circumvent this problem, since in that representation the first-derivative coupling element is minimized. It has been shown[32,33] that in general a perfect diabatic basis that makes that first term vanish for all nuclear geometries does not exist for a polyatomic system, and hence a finite part of the first-derivative coupling cannot be totally removed even in the diabatic representation. This part is referred to in literature as the *nonremovable* part. For systems having a conical intersection, $\mathbf{W}_{1,2}^{(1)\mathrm{ad}}(\mathbf{q})$ has a singularity at conical intersection geometries.[34] This singularity along with some finite part of the coupling is *removable* upon an adiabatic to diabatic transformation and is hence referred to as the *removable* part. Mead and Truhlar[33] have shown how to calculate the *removable* part, but their approach is difficult to implement.[35] Over the years, a number of formalisms involving (quasi)diabatic basis have also been put forward.[35–45]

This paper focuses on the calculation of high quality *ab initio* ground and first-excited electronic energies and the first-derivative couplings between them. The second-derivative couplings are generally assumed to be negligible as compared to the other terms in the Hamiltonian [Eq. (1)], except at the conical intersection.[46] These accurate energies and first-derivative couplings will be used for transforming the two-state adiabatic problem expressed by Eq. (1) to a (quasi)diabatic representation and will be incorporated into the quantum scattering formalism to calculate the effect of conical intersections on the dynamics of the chemical reactions at energies for which a minimum of two electronic states are required to obtain accurate results.

The $H+H_2$ system is being used for this work because it is the simplest of the chemical reactions for which the concurrent bond breaking and bond formation can be studied in detail both experimentally and theoretically. Many quantum scattering calculations have been performed on this system.[14,15,47–50] The equilateral triangle (C_{3v}) configuration of H_3 corresponds to a conical intersection between the ground and the first-excited electronic states of the system. This conical intersection induces a GP that is important in studying the reactive scattering in the ground state.[12,14–18,51,52] With the breakdown of the one electronic state Born–Oppenheimer approximation near 2.75 eV, which corresponds to the minimum of the first-excited PES,[53] both surfaces must be used in a scattering calculation for an ac-

curate result to be obtained. Such two-state calculations should be performed and compared with the recent quantum scattering calculations[14,15] done with and without the inclusion of the GP effect. This comparison is expected to provide an upper limit to the energy at which the ground state PES by itself, with an incorporation of the GP effect, is capable of furnishing a quantitative description of the reaction dynamics of the H_3 system and its isotopomers.

In this paper, we present the first-derivative nonadiabatic couplings between the ground and the first-excited PESs for the $H+H_2$ system obtained from high quality *ab initio* wave functions and analytic gradient techniques over the entire nuclear internal configuration space. We also present a fit to the corresponding ground and first-excited electronic PESs and analyze the regions of that space for which the first-derivative couplings could affect the dynamics of the $H+H_2$ reaction. For comparison, we also present the first-derivative couplings and the lowest two electronic PESs obtained analytically from the double many-body expansion (DMBE) method of Varandas *et al.*,[54] as the DMBE couplings are designed to be accurate only in the vicinity of the conical intersection.

In Sec. II, we describe the methods used to obtain the first-derivative couplings and introduce their contour integrals. In Sec. III, we present a fit to the *ab initio* energies corresponding to the lowest two electronic PESs and compare them to the DMBE ones. We present and compare the *ab initio* and DMBE first-derivative couplings in Sec. IV, which is concluded by an analysis of the contour integrals of the *ab initio* couplings. In Sec. V, we provide a summary and conclusions.

II. THEORY AND NUMERICAL METHODS

A. *Ab initio* couplings and electronic energies

The first-derivative couplings are determined using an analytic gradient technique summarized in Ref. 55. This technique is a significant improvement over the finite-difference techniques introduced previously[25,56–59] and has been used recently in a number of problems to obtain electronic energies and first-derivative couplings.[42,60–63] Using it, the first-derivative couplings are first evaluated in terms of six atom-centered displacements[55] in the H_3 molecular plane and then transformed to standard internal mass-scaled Jacobi coordinates $(R_\lambda, r_\lambda, \gamma_\lambda)$. In addition to the derivative couplings associated with these coordinates, the coupling due to rotation in the molecular plane is also determined. This rotational coupling must equal the interstate matrix element of the z component of total electronic orbital angular momentum operator, L_z^e.[64,65] This equivalence provides a measure of the precision of the derivative couplings presented in this paper and the two approaches agree to 1×10^{-6} bohr^{-1}.

In this work, the first-derivative couplings and the ground (E_1) and first-excited (E_2), electronic PESs for H_3 were determined on a grid of 784 geometry points picked in the symmetrized hyperspherical coordinates $(\mathbf{q}{:}\rho,\theta,\phi_\lambda)$ used previously[12,14] and defined in detail in Sec. III. The adiabatic wave functions, first-derivative couplings, and electronic energies were determined from second-order configuration interaction (CI)[66–68] wave functions based on a three electron, three orbital, active space. The molecular orbitals were determined from a complete active space[69–71] state-averaged multiconfiguration self-consistent field[72,73] procedure in which two $^2A'$ states were averaged with weights (0.505,0.495) based on $(6s3p1d)$ contracted Gaussian basis sets on the hydrogens.

After being evaluated in nuclear mass-scaled Jacobi coordinates as mentioned previously, the first-derivative couplings are transformed to the $\mathbf{q}$ coordinates $(\rho,\theta,\phi_\lambda)$ to obtain the first-derivative coupling vector,

$$\mathbf{W}_{1,2}^{(1)\mathrm{ad}}(\mathbf{q}) = \langle \psi_1^{\mathrm{ad}}(\mathbf{r};\mathbf{q}) | \nabla_{\mathbf{q}} \psi_2^{\mathrm{ad}}(\mathbf{r};\mathbf{q}) \rangle_{\mathbf{r}}, \tag{8}$$

whose components in the ρ, θ, and ϕ_λ unit vector directions are defined as

$$W_{1,2,\rho}^{(1)\mathrm{ad}}(\rho,\theta,\phi_\lambda) = \left\langle \psi_1^{\mathrm{ad}}(\mathbf{r};\rho,\theta,\phi_\lambda) \left| \frac{\partial}{\partial\rho} \psi_2^{\mathrm{ad}}(\mathbf{r};\rho,\theta,\phi_\lambda) \right\rangle_{\mathbf{r}}, \tag{9}$$

$$W_{1,2,\theta}^{(1)\mathrm{ad}}(\rho,\theta,\phi_\lambda) = \left\langle \psi_1^{\mathrm{ad}}(\mathbf{r};\rho,\theta,\phi_\lambda) \left| \frac{1}{\rho}\frac{\partial}{\partial\theta} \psi_2^{\mathrm{ad}}(\mathbf{r};\rho,\theta,\phi_\lambda) \right\rangle_{\mathbf{r}}, \tag{10}$$

$$W_{1,2,\phi_\lambda}^{(1)\mathrm{ad}}(\rho,\theta,\phi_\lambda) = \left\langle \psi_1^{\mathrm{ad}}(\mathbf{r};\rho,\theta,\phi_\lambda) \left| \frac{1}{\rho\sin\theta}\frac{\partial}{\partial\phi_\lambda} \psi_2^{\mathrm{ad}}(\mathbf{r};\rho,\theta,\phi_\lambda) \right\rangle_{\mathbf{r}}. \tag{11}$$

The values of the $\mathbf{q}$ coordinates $(\rho,\theta,\phi_\lambda)$ are limited to the ranges

$$0\leqslant\rho<\infty, \quad 0\leqslant\theta\leqslant\pi/2, \quad 0\leqslant\phi_\lambda<2\pi. \tag{12}$$

$\theta=0°$ corresponds to conical intersection geometries. As seen from Eq. (11) and the behavior of $\psi_1^{\mathrm{ad}}(\mathbf{r};\rho,\theta,\phi_\lambda)$ and $\psi_2^{\mathrm{ad}}(\mathbf{r};\rho,\theta,\phi_\lambda)$ in the vicinity of the conical intersection [see Eq. (116) of Ref. 12], $W_{1,2,\phi_\lambda}^{(1)\mathrm{ad}}$ has a pole at those geometries.

A three-dimensional cubic spline[74] interpolation of the components of the first-derivative coupling vector is performed using all 784 geometries. The vector resulting from this interpolation is presented and discussed in Sec. IV. The adiabatic electronic energies for the ground and first-excited states are fitted by a method that will be described in Sec. III.

According to Mead and Truhlar,[33] the first-derivative coupling vector can be partitioned (using the Helmholtz decomposition theorem[75]) as

$$\mathbf{W}_{1,2}^{(1)\mathrm{ad}}(\mathbf{q}) = \mathbf{W}_{1,2,\mathrm{lon}}^{(1)\mathrm{ad}}(\mathbf{q}) + \mathbf{W}_{1,2,\mathrm{tra}}^{(1)\mathrm{ad}}(\mathbf{q}), \tag{13}$$

where $\mathbf{W}_{1,2,\mathrm{lon}}^{(1)\mathrm{ad}}(\mathbf{q})$ is the curl-free longitudinal (*removable*) part and $\mathbf{W}_{1,2,\mathrm{tra}}^{(1)\mathrm{ad}}(\mathbf{q})$ is the divergence-free transverse (*nonremovable*) part of the coupling vector. Although $\mathbf{W}_{1,2}^{(1)\mathrm{ad}}(\mathbf{q})$ is singular, the Helmholtz theorem is still valid in this case because the singularity can be removed analytically[76] from $W_{1,2,\phi_\lambda}^{(1)\mathrm{ad}}$. For a strictly diabatic two electronic state basis, $\mathbf{W}_{1,2,\mathrm{tra}}^{(1)\mathrm{ad}}(\mathbf{q})$ is identically zero. In the present two-adiabatic-electronic-state approximation, $\mathbf{W}_{1,2,\mathrm{tra}}^{(1)\mathrm{ad}}(\mathbf{q})$ is not zero due to the presence of contributions to $\mathbf{W}_{1,2}^{(1)\mathrm{ad}}(\mathbf{q})$ from other nonnegligible derivative couplings with states outside this two-

TABLE I. Switching function parameters.[a]

Parameter	$1\,^2A'$	$2\,^2A'$
a_n (bohr)	0.00	2.00
γ_n (bohr^{-1})	0.17	0.20

[a]These parameters are used for S_n, as described in Eqs. (22)–(25).

state space [see Eq. (28) of Ref. 33]. Since $\mathbf{W}^{(1)\mathrm{ad}}_{1,2,\mathrm{lon}}(\mathbf{q})$ is curl free, an angular potential $\beta(\mathbf{q})$ exists for which

$$\mathbf{W}^{(1)\mathrm{ad}}_{1,2,\mathrm{lon}}(\mathbf{q})=\boldsymbol{\nabla}_{\mathbf{q}}\beta(\mathbf{q}). \tag{14}$$

This equation can be solved by integration along paths $\mathcal{L}$ in the nuclear configuration space,[32,42,77]

$$\beta(\mathbf{q})=\int_{\mathcal{L}\,\mathbf{q_0}}^{\mathbf{q}}\mathbf{W}^{(1)\mathrm{ad}}_{1,2,\mathrm{lon}}(\mathbf{q}')\cdot d\mathbf{q}', \tag{15}$$

where $\mathbf{q_0}$ is a point along $\mathcal{L}$ at which we take $\beta(\mathbf{q_0})=0$. β defined in this way is a particular diabatization angle that transforms an adiabatic basis to a diabatic basis. It should be noted that because of Eq. (14), this integral depends on $\mathbf{q}$ and $\mathbf{q_0}$, but not on the path $\mathcal{L}$. In addition, if the integral in Eq. (15) is carried along a closed loop enclosing one or no conical intersections, due to the geometric phase theorem β should change by π or zero, respectively.[11,42,60] We can define another angular potential $\Phi(\mathbf{q},\mathbf{q_0};\mathcal{L})$ corresponding to the $\mathbf{W}^{(1)\mathrm{ad}}_{1,2}(\mathbf{q})$ analog of Eq. (15) by

$$\Phi(\mathbf{q},\mathbf{q_0};\mathcal{L})=\int_{\mathcal{L}\,\mathbf{q_0}}^{\mathbf{q}}\mathbf{W}^{(1)\mathrm{ad}}_{1,2}(\mathbf{q}')\cdot d\mathbf{q}'. \tag{16}$$

This angle is called the open path phase if $\mathbf{q}\neq\mathbf{q_0}$.[78] It is also convenient to define the corresponding closed path phase Φ_{T}, called the topological phase:[79]

$$\Phi_{\mathrm{T}}(\mathcal{L})=\oint_{\mathcal{L}}\mathbf{W}^{(1)\mathrm{ad}}_{1,2}(\mathbf{q}')\cdot d\mathbf{q}'. \tag{17}$$

Since $\mathbf{W}^{(1)\mathrm{ad}}_{1,2}(\mathbf{q})$ does not in general satisfy Eq. (14), these path integrals are no longer independent of the path $\mathcal{L}$. It is also convenient to define the angle $\eta(\mathcal{L})$ by

$$\eta(\mathcal{L})=\Phi_{\mathrm{T}}(\mathcal{L})-p\pi, \tag{18}$$

where $p=0$ if $\mathcal{L}$ does not enclose any conical intersection and $p=1$ if it encloses one conical intersection. This angle is the closed path integral of the transverse part of the first-derivative coupling. A necessary but insufficient condition for the first-derivative coupling to be purely longitudinal is that $\eta(\mathcal{L})$ should vanish.[76] Since conical intersections produce large derivative couplings, large $\eta(\mathcal{L})$ have been interpreted in the past as indicating the existence of conical intersections with the first excluded state[42] or even to locate such intersections.[80] In Sec. IV, we present values of the topological phase between the first two states of H_3 over the entire nuclear configuration space and discuss the results.

TABLE II. Coefficients[a] $c_{1,ijk}$ and $c_{2,ijk}$ corresponding to E_1^{DSP} and E_2^{DSP}, respectively [as defined in Eq. (22)].[b]

i	j	k	$c_{1,ijk}$	$c_{2,ijk}$
0	0	0	0.3699	−0.2274
1	0	0	−0.4927	0.0255
2	0	0	0.4726	0.0996
1	1	0	0.0237	0.2025
3	0	0	−0.2590	−0.2606
2	1	0	0.1258	0.1934
1	1	1	−0.4795	−1.2400
4	0	0	0.0398	0.0845
3	1	0	−0.0156	0.0075
2	1	1	0.0299	0.2397
2	2	0	−0.0162	−0.2428
5	0	0	−0.0018	−0.0070
4	1	0	0.0006	−0.0155
3	2	0	0.0005	0.0332
2	2	1	−0.0006	−0.0378
3	1	1	−0.0009	−0.0044
6	0	0	⋯	0.0000
5	1	0	⋯	0.0013
4	2	0	⋯	−0.0015
3	3	0	⋯	−0.0013
3	2	1	⋯	−0.0001
4	1	1	⋯	0.0006
2	2	2	⋯	0.0062

[a]$c_{1,ijk}=c_{1,jki}=c_{1,kij}$ and $c_{2,ijk}=c_{2,jki}=c_{2,kij}$.
[b]With these $c_{n,ijk}$ coefficients used in Eq. (22) and R_{AB}, R_{BC}, R_{CA} given in bohr, the E_n^{DSP} are given in eV and are referred to the minimum of an isolated H_2 molecule as the origin of energy.

B. DMBE couplings and electronic energies

Varandas *et al.*[54] have reported an analytical representation of the lowest electronic PES ($1\,^2A'$) of $H+H_2$ based on the DMBE method. For the DMBE fit, they used 267 *ab initio* points of Liu and Siegbahn,[81,82] 31 points from Blomberg and Liu,[83] and 18 new *ab initio* points. Their *ab initio* calculations employed a primitive $(9s3p1d)$ basis set contracted to $[4s3p1d]$. They first performed a complete-active-space-self-consistent-field calculation[69] with the three active orbitals to obtain eight configurations. It was followed by a multireference CI calculation with all single and double excitations out of that eight configuration reference space (MR-CISD). The fundamental form used for the DMBE fit has correct analytical properties[84–87] for a PES exhibiting a C_{3v} conical intersection and is analytically continued to the first-excited electronic PES ($2\,^2A'$). In the process, it yields a good representation of the first-derivative couplings in the vicinity of the conical intersection. In fact, it gives the leading terms of the longitudinal part of the first-derivative coupling vector, $\mathbf{W}^{(1)\mathrm{ad}}_{1,2,\mathrm{lon}}(\mathbf{q})$. Varandas *et al.*[54] also mention that these leading terms (of the longitudinal part) can be determined from the adiabatic PESs, but the transverse part $[\mathbf{W}^{(1)\mathrm{ad}}_{1,2,\mathrm{tra}}(\mathbf{q})]$ cannot be completely determined. Besides, in the vicinity of the conical intersection, $\mathbf{W}^{(1)\mathrm{ad}}_{1,2,\mathrm{lon}}(\mathbf{q})$ diverges but the $\mathbf{W}^{(1)\mathrm{ad}}_{1,2,\mathrm{tra}}(\mathbf{q})$ part stays finite and small. Hence, the leading terms that provide the longitudinal part give a good representation of the first-derivative couplings in the vicinity of the conical intersection.

Using the DMBE method, it has been shown[54,85] that the

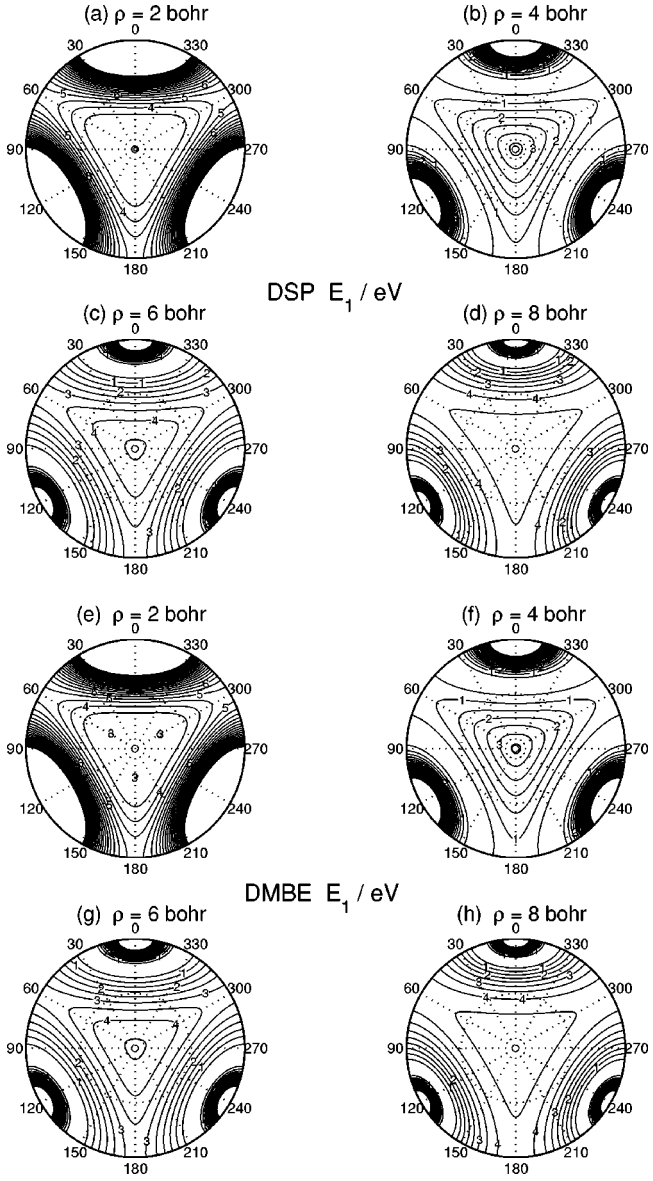

FIG. 1. Ground electronic state (E_1) energy contours in eV for the H_3 system in an equatorial view (see the text for the definition): (a) DSP E_1 at $\rho=2$ bohr, (b) DSP E_1 at $\rho=4$ bohr, (c) DSP E_1 at $\rho=6$ bohr, (d) DSP E_1 at $\rho=8$ bohr, (e) DMBE E_1 at $\rho=2$ bohr, (f) DMBE E_1 at $\rho=4$ bohr, (g) DMBE E_1 at $\rho=6$ bohr, (h) DMBE E_1 at $\rho=8$ bohr. The solid circle depicts collinear geometries ($\theta=90°$) and the dotted circles are lines of constant θ. The radial dotted lines correspond to the constant values of ϕ_λ, in degrees, displayed outside the solid circle.

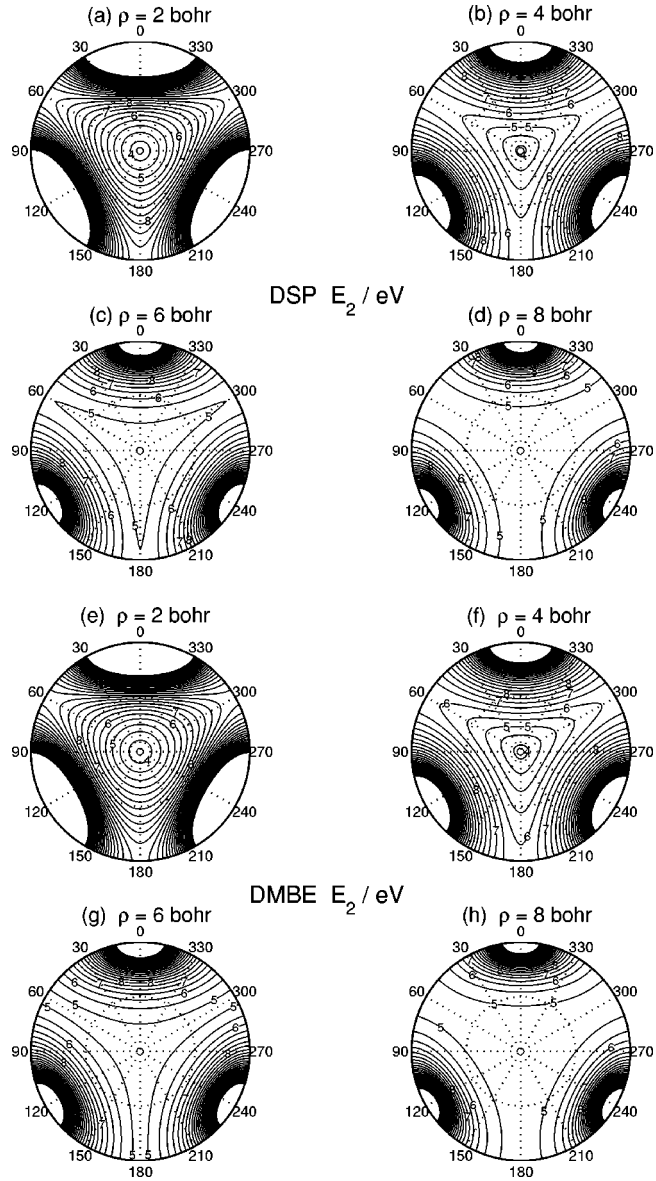

FIG. 2. First-excited electronic state (E_2) energy contours in eV for the H_3 system in an equatorial view (see the text for the definition): (a) DSP E_2 at $\rho=2$ bohr, (b) DSP E_2 at $\rho=4$ bohr, (c) DSP E_2 at $\rho=6$ bohr, (d) DSP E_2 at $\rho=8$ bohr, (e) DMBE E_2 at $\rho=2$ bohr, (f) DMBE E_2 at $\rho=4$ bohr, (g) DMBE E_2 at $\rho=6$ bohr, (h) DMBE E_2 at $\rho=8$ bohr. The solid circle depicts collinear geometries ($\theta=90°$) and the dotted circles are lines of constant θ. The radial dotted lines correspond to the constant values of ϕ_λ, in degrees, displayed outside the solid circle.

longitudinal part and hence the total DMBE first-derivative coupling vector can be approximated (assuming the transverse part to be zero over the entire configuration space) as

$$\mathbf{W}_{1,2}^{(1)\mathrm{ad,DMBE}}(\mathbf{q}) \sim \mathbf{W}_{1,2,\mathrm{lon}}^{(1)\mathrm{ad,DMBE}}(\mathbf{q}) = \boldsymbol{\nabla}_{\mathbf{q}} \beta^{\mathrm{DMBE}}(\mathbf{q}), \quad (19)$$

where

$$\beta^{\mathrm{DMBE}}(\mathbf{q}) = \frac{1}{2}\left[\phi_\lambda - \tan^{-1}\frac{g_0(\rho)\sin\theta\sin 3\phi_\lambda}{f_0(\rho)+g_0(\rho)\sin\theta\cos 3\phi_\lambda + f_1(\rho)\sin^2\theta}\right]. \quad (20)$$

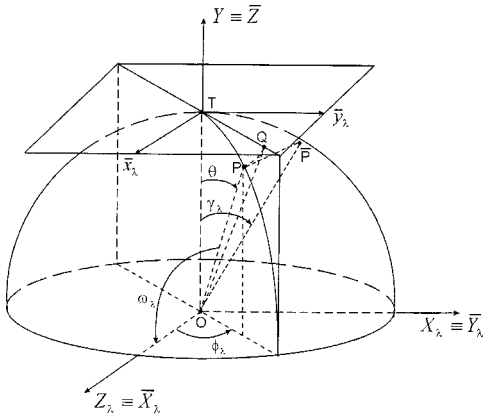

FIG. 3. Mapping of the point P of a constant ρ hemisphere in the $OX_\lambda YZ_\lambda$ space onto a point Q on a plane tangent to that hemisphere at the intersection T of the OY axis with it, such that the length of the arc(TP)=TQ. The point P has θ,ϕ_λ polar angles in the $OX_\lambda YZ_\lambda$ space and $\omega_\lambda,\gamma_\lambda$ in the $O\bar{X}_\lambda\bar{Y}_\lambda\bar{Z}$ space. $\bar{P}$ is the projection of point P on the $OX_\lambda Y$ plane.

Equations (19) and (20) have been obtained in our hyperspherical coordinates by replacing s by $\sin\theta$ and ϕ by our ϕ_λ in Eq. (48) of Ref. 54. $g_0(\rho)$, $f_0(\rho)$, and $f_1(\rho)$ are some factors that depend only on the hyperradius ρ. The original DMBE code was used in this work to obtain these longitudinal couplings and the two lowest PESs for H_3. In the vicinity of the conical intersection, these longitudinal couplings are expected to be quite close to the *ab initio* first-derivative couplings. Using this criterion, a systematic mismatch in sign was found in those couplings and was removed by flipping the sign of $g_0(\rho)$ in the DMBE code. These DMBE couplings are presented and compared with the *ab initio* ones in Sec. IV. In Sec. III, the two lowest DMBE PESs for H_3 are compared to the PESs obtained from the fits of the *ab initio* energies.

III. *AB INITIO* AND DMBE ELECTRONIC ENERGIES

A. Fitting method

Any PES fitting procedure is expected to be reasonably simple, result in good agreement with the *ab initio* data, and have a physically realistic mathematical form to minimize the number of *ab initio* geometries needed to obtain a surface with correct features and topology.[88,89] We have used a DMBE plus single-polynomial (DSP) fitting method based on the recent[90] generalized London–Eyring–Polanyi–Sato double-polynomial method as it satisfies most of the above-mentioned criteria for fitting methods. The DSP method uses data from the DMBE fit to the lowest two adiabatic electronic PESs for H_3. Since the original DMBE fit is explained in detail in Ref. 54, we will only describe the DSP method here.

The DSP mathematical form used for the lowest two PESs for H_3 is the sum of two terms,

$$E_n^{\mathrm{DSP}} = E_n^{\mathrm{DMBE}} + E_n^{\mathrm{POLY}}, \tag{21}$$

where $n=1$ or 2 for the ground or first-excited PES respectively. The first term is the DMBE potential,[54] as it gives a good physical description of the two PESs. The second term is a single high-order polynomial multiplied by a switching function and modifies the initial DMBE potential to provide greater accuracy. With the three H atoms in H_3 labeled A_α, A_β, or A_γ, this polynomial term is defined by

$$E_n^{\mathrm{POLY}} = S_n(\mathbf{q})\left(\sum_{i+j+k=0}^{t_n} c_{n,ijk}(R_{\alpha\beta}-a_n)^i (R_{\beta\gamma}-a_n)^j (R_{\gamma\alpha}-a_n)^k \right), \tag{22}$$

where $R_{\lambda\nu}$ is the distance between A_λ and A_ν ($\lambda\nu=\alpha\beta,\beta\gamma,\gamma\alpha$). The $c_{n,ijk}$ are coefficients and $S_n(\mathbf{q})$ are the switching functions. The switching function S is used to turn the single polynomial in E_n^{POLY} on and off in different regions of the internal nuclear configuration space. Terms up to fifth order ($t_1=5$) are used in the above-mentioned polynomial for the ground state PES and up to sixth order ($t_2=6$) for the first-excited PES. The sum extends over all possible sets of i,j,k satisfying the condition $i+j+k\leqslant t_n$. The switching function S is defined by

$$S_n(\mathbf{q}) = s(y_{n,\alpha\beta})s(y_{n,\beta\gamma})s(y_{n,\gamma\alpha}), \tag{23}$$

where

$$s(y_{n,\lambda\nu}) = 1-\tanh(y_{n,\lambda\nu}), \tag{24}$$

in which

$$y_{n,\lambda\nu} = \gamma_n(R_{\lambda\nu}-a_n), \quad \lambda\nu=\alpha\beta,\beta\gamma,\gamma\alpha. \tag{25}$$

The $c_{n,ijk}$, a_n, and γ_n are variational parameters determined by the fitting method. The $s(y_{n,\lambda\nu})$ terms in Eq. (24) turn the E_n^{POLY} term off for the asymptotic geometries. As a result, the asymptotic regions of the PESs have the correct diatomic behavior, included in the E_n^{DMBE} term. The slope parameter, γ_n, having dimensions of a reciprocal length controls how rapidly E_n^{POLY} is made to vanish, whereas a_n is a reference internuclear distance.

The DSP mathematical form is fitted to the *ab initio* data using a *linear* least-squares method to obtain the set of variational parameters (a_n and γ_n) that minimize the root-mean-square (rms) error. Using an initial estimate of the parameters, the $c_{n,ijk}$ and the corresponding rms error ϵ are determined by a linear variational procedure. a_n and γ_n are then varied and the determination of $c_{n,ijk}$ and ϵ is repeated until that error is minimized. This procedure is carried out for both the ground and first-excited PESs, and the resulting PESs are examined with the help of equipotential contour plots in the corresponding two-internuclear-distance Cartesian space at fixed bond angles for any spurious features in these PESs. No such features were detected. The fitted ground PES $1\,^2A'$ (E_1^{DSP}) has a rms error with respect to the *ab initio* data of 0.31 kcal/mol and the corresponding error for the fitted first-excited PES $2\,^2A'$ (E_2^{DSP}) is 1.12 kcal/mol. The optimized parameters (a_n and γ_n) are given in Table I and the corresponding optimized coefficients ($c_{n,ijk}$) are given in Table II. These fitted DSP PESs are also examined in hyperspherical coordinates with the help of equipotential contour plots at fixed hyperradii, as discussed in Sec. III B and compared with the corresponding contour plots for the DMBE PESs.

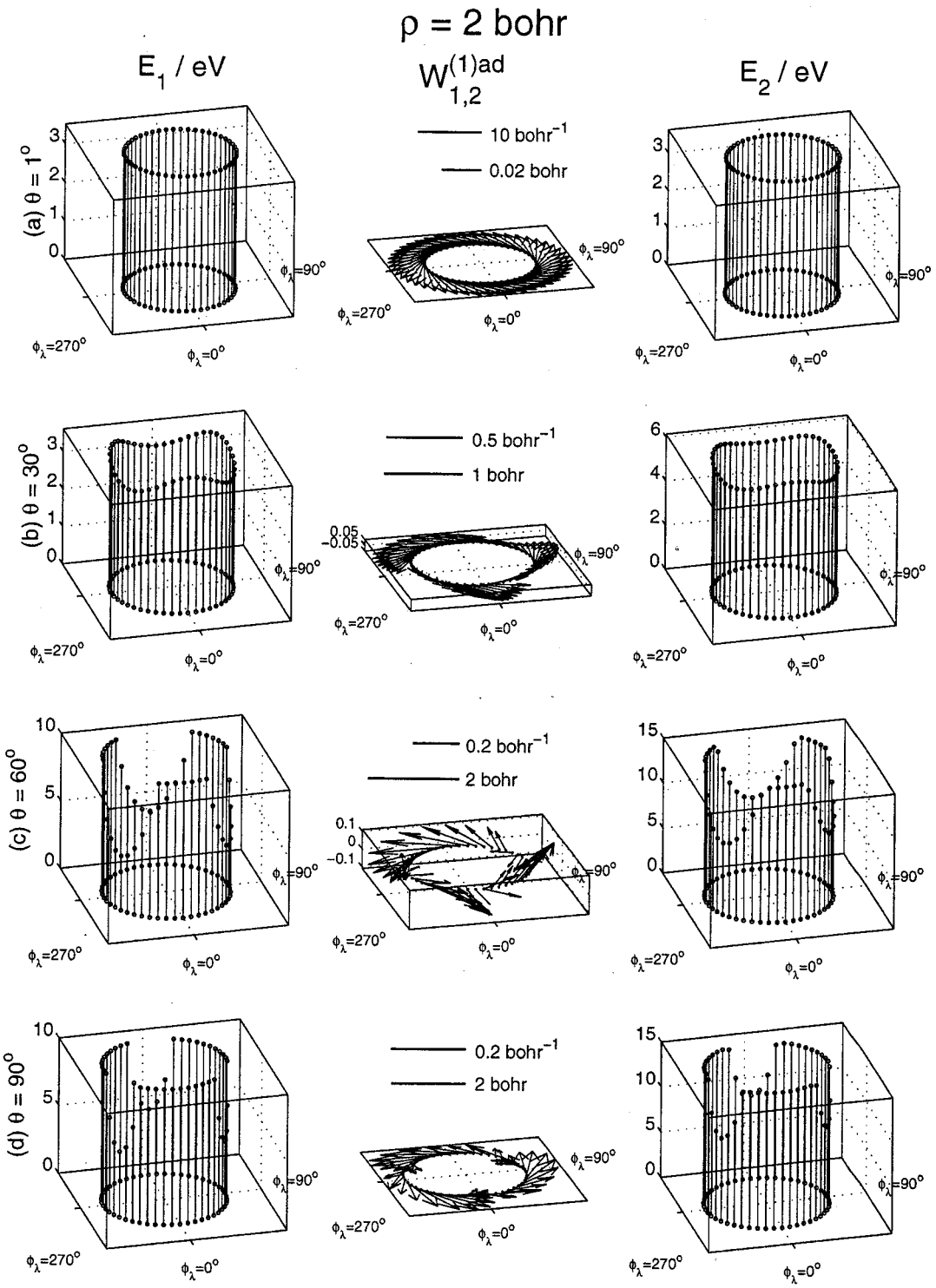

FIG. 4. *Ab initio* nonadiabatic coupling vector, $\mathbf{W}_{1,2}^{(1)\mathrm{ad}}$, ground state energy ($E_1$), and first-excited state energy (E_2) for $\rho=2$ bohr and (a) $\theta=1°$; (b) $\theta=30°$; (c) $\theta=60°$; (d) $\theta=90°$ (collinear). The scale in bohr^{-1} refers to coupling vectors, and that in bohr to the Cartesian coordinates associated with the middle column plots (see Sec. IV A).

B. DSP and DMBE potential energy surfaces

Equatorial projection plots (Figs. 1 and 2) of potential energy surfaces in internal symmetrized hyperspherical coordinates $(\rho,\theta,\phi_\lambda)$[12,14,91] provide useful information for reactive scattering calculations that use these coordinates. These plots are obtained as follows. Let the arrangement channel $A_\lambda+A_\nu A_\kappa$ be called the λ arrangement channel, where $\lambda\nu\kappa$ is a cyclic permutation of $\alpha\beta\gamma$. Let $\mathbf{R}'_\lambda,\mathbf{r}'_\lambda$ be the Jacobi vectors associated with this arrangement channel, where $\mathbf{r}'_\lambda$ is the vector from A_ν to A_κ and $\mathbf{R}'_\lambda$ the vector from the center of mass of $A_\nu A_\kappa$ to A_λ. Let $\mathbf{R}_\lambda$, $\mathbf{r}_\lambda$ be the corresponding mass-scaled Jacobi coordinates[91–95] defined by

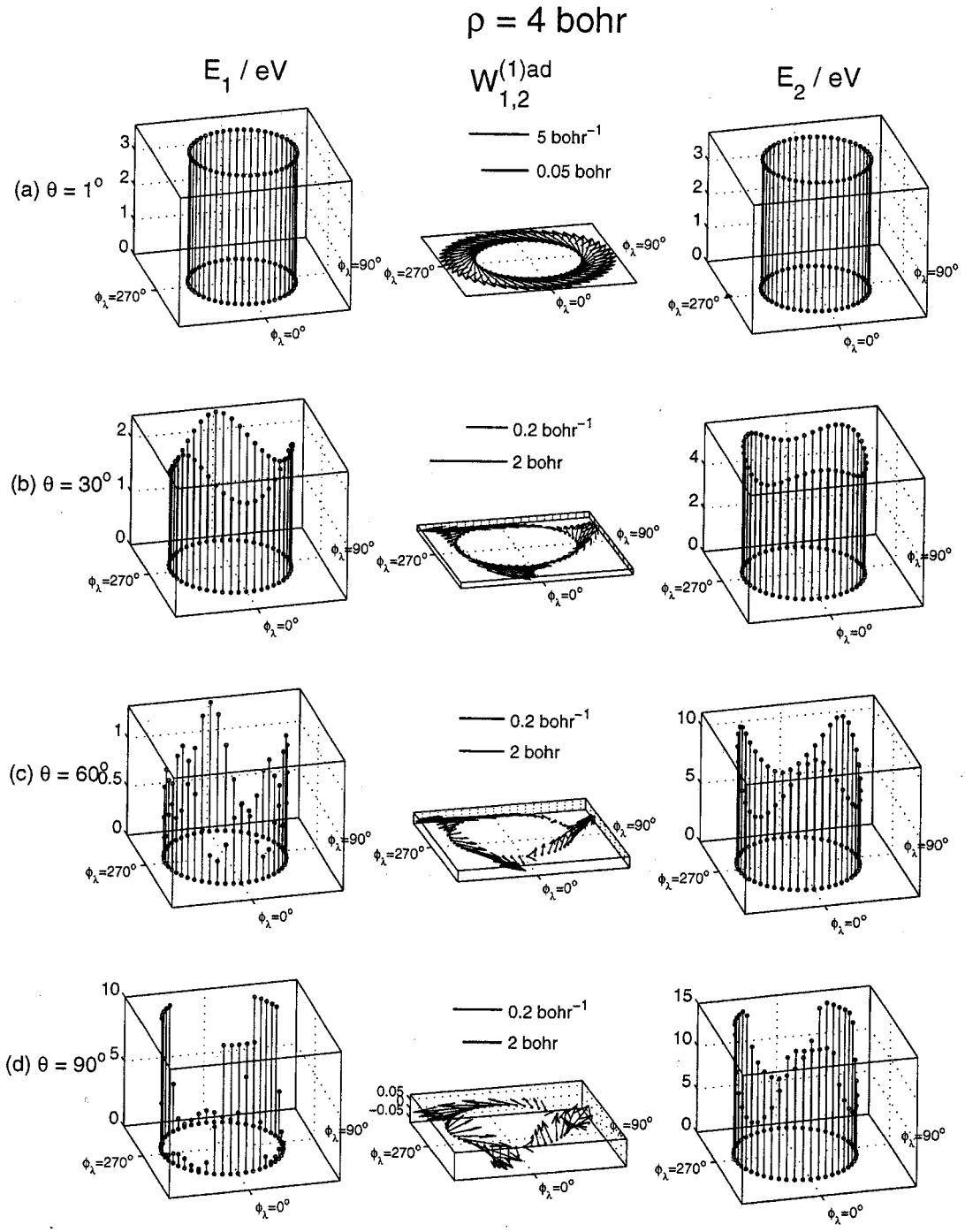

FIG. 5. Same as Fig. 4 for $\rho=4$ bohr.

$$\mathbf{R}_\lambda=\left(\frac{\mu_{\lambda,\nu\kappa}}{\mu}\right)^{1/2}\mathbf{R}'_\lambda,\quad \mathbf{r}_\lambda=\left(\frac{\mu_{\nu\kappa}}{\mu}\right)^{1/2}\mathbf{r}'_\lambda, \tag{26}$$

where $\mu_{\nu\kappa}$ is the reduced mass of $A_\nu A_\kappa$, $\mu_{\lambda,\nu\kappa}$ the reduced mass of the $A_\lambda, A_\nu A_\kappa$ pair, and μ the system's overall reduced mass given by

$$\mu=\left(\frac{m_\alpha m_\beta m_\gamma}{m_\alpha+m_\beta+m_\gamma}\right)^{1/2},$$

m_λ being the mass of atom A_λ $(\lambda=\alpha,\beta,\gamma)$. We now define a set of symmetrized hyperspherical coordinates $\rho,\omega_\lambda,\gamma_\lambda$ (Refs. 91 and 96), by

$$\rho=(R_\lambda^2+r_\lambda^2)^{1/2} \tag{27}$$

and

$$R_\lambda=\rho\cos\frac{\omega_\lambda}{2},\quad r_\lambda=\rho\sin\frac{\omega_\lambda}{2},\quad 0\leqslant\omega_\lambda\leqslant\pi, \tag{28}$$

where ρ is independent of the arrangement channel.[92,93] The corresponding internal configuration space Cartesian coordinates are defined by

$$X_\lambda=\rho\sin\omega_\lambda\cos\gamma_\lambda, \tag{29}$$

$$Y=\rho\sin\omega_\lambda\sin\gamma_\lambda, \tag{30}$$

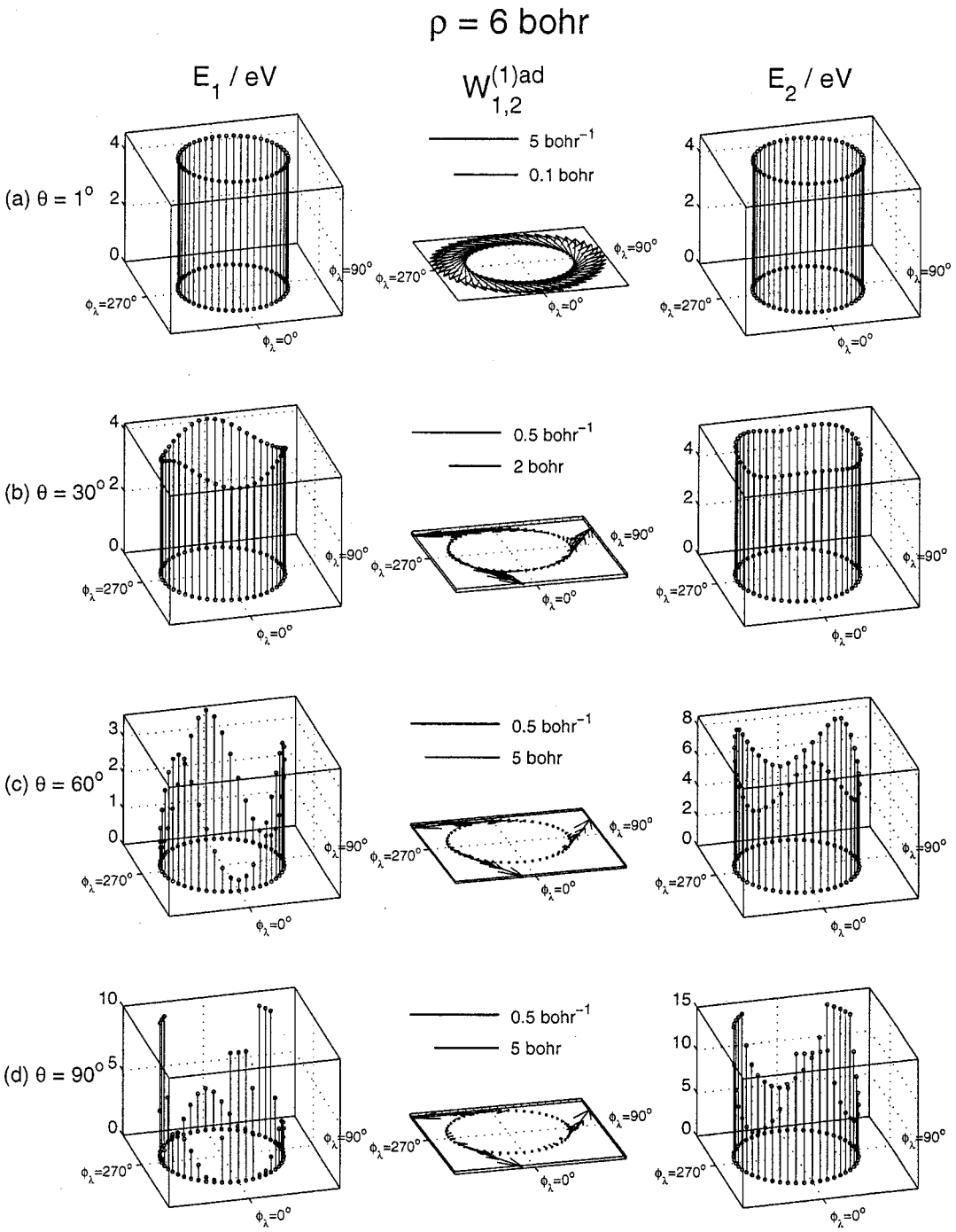

FIG. 6. Same as Fig. 4 for $\rho=6$ bohr.

$$Z_\lambda = \rho \cos \omega_\lambda , \tag{31}$$

where γ_λ is the angle between $\mathbf{R}_\lambda$ and $\mathbf{r}_\lambda$ (or $\mathbf{R}'_\lambda$ and $\mathbf{r}'_\lambda$) in the 0 to π range and $\omega_\lambda, \gamma_\lambda$ are the polar angles of a point in this space. The alternate internal configuration space symmetrized hyperspherical coordinates θ, ϕ_λ are defined as the polar angles associated with the interchanged axes $\mathsf{O}\overline{X}_\lambda = \mathsf{O}Z_\lambda$, $\mathsf{O}\overline{Y}_\lambda = \mathsf{O}X_\lambda$, and $\mathsf{O}\overline{Z}_\lambda = \mathsf{O}Y_\lambda$ for which we have

$$\overline{X}_\lambda = Z_\lambda = \rho \sin\theta \cos\phi_\lambda , \tag{32}$$

$$\overline{Y}_\lambda = X_\lambda = \rho \sin\theta \sin\phi_\lambda , \tag{33}$$

$$\overline{Z} = Y = \rho \cos\theta, \tag{34}$$

with θ and ϕ_λ limited to the ranges given in Eq. (12).

The coordinates used for Figs. 1 and 2 correspond to a mapping[91,97] of the points P of a constant ρ hemisphere in the $\mathsf{O}X_\lambda Y Z_\lambda$ space onto a plane tangent to that hemisphere at the intersection T of the $\mathsf{O}Y$ axis with it (Fig. 3). Let $\mathsf{T}\overline{x}_\lambda$ and $\mathsf{T}\overline{y}_\lambda$ be, respectively, the intersection of the $\mathsf{O}Z_\lambda Y$ and $\mathsf{O}X_\lambda Y$ planes with that tangent plane. The corresponding $\overline{x}_\lambda$ and $\overline{y}_\lambda$ of the map Q of the point P onto the tangent plane are then

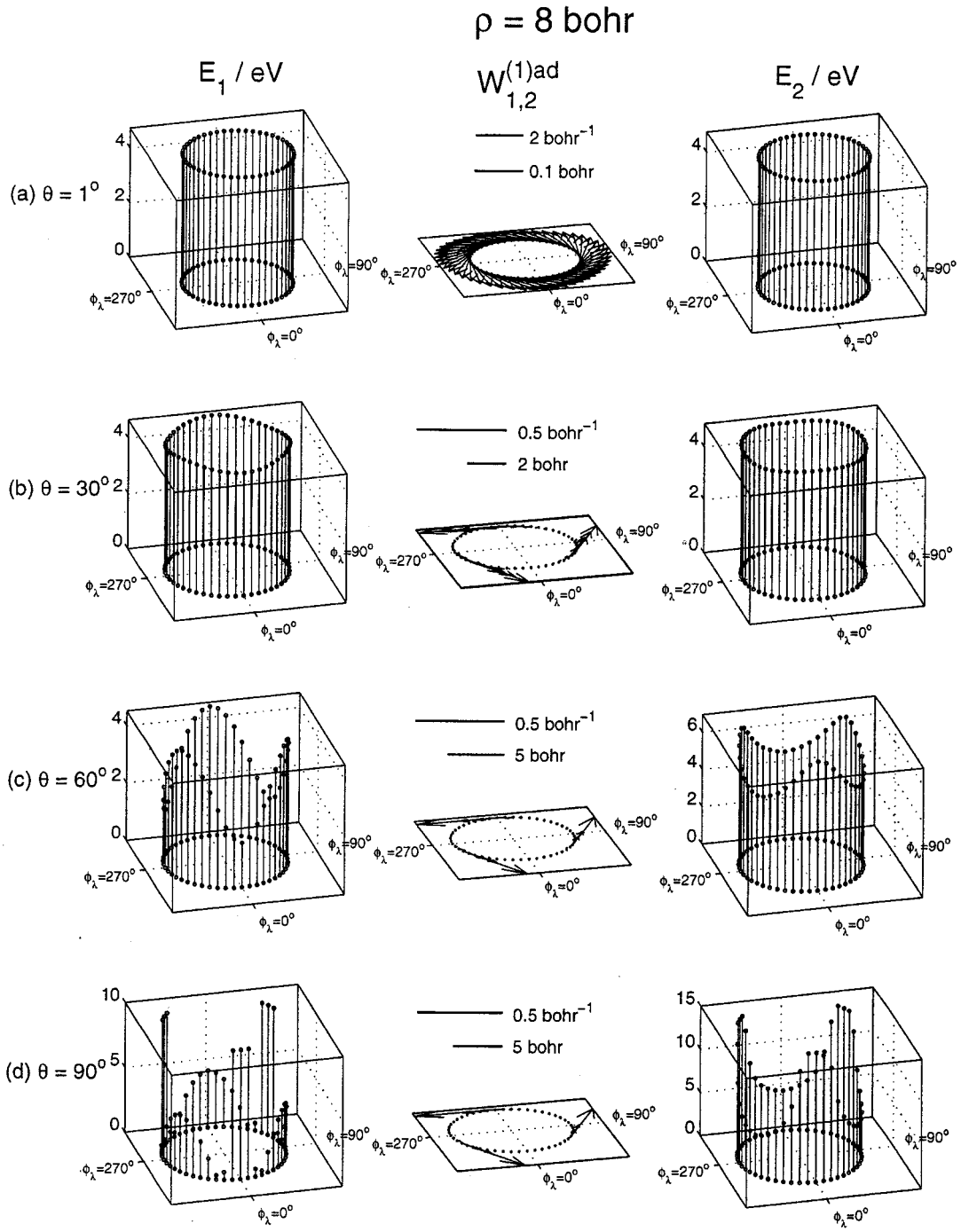

FIG. 7. Same as Fig. 4 for $\rho=8$ bohr.

$$\overline{x_\lambda}=\rho\theta\cos\phi_\lambda\,, \tag{35}$$

$$\overline{y_\lambda}=\rho\theta\sin\phi_\lambda\,. \tag{36}$$

This mapping of P onto Q is not a perpendicular projection, but is one in which the length of the arc PT of the circle of center O on the constant ρ hemisphere is equal to the length of the straight line TQ on the tangent plane.

To obtain such maps, we start out with a configuration of the molecule defined by the three internuclear distances $R_{\alpha\beta}$, $R_{\beta\gamma}$, and $R_{\gamma\alpha}$ and then calculate R'_λ (the magnitude of $\mathbf{R}'_\lambda$), r'_λ (the magnitude of $\mathbf{r}'_\lambda$), and γ_λ. From the first two we calculate the mass-scaled distances R_λ and r_λ and then, with the help of Eqs. (27) and (28) we obtain ρ and ω_λ. Using Eqs. (29)–(34) and (12) we then calculate θ and ϕ_λ and finally we obtain $\overline{x_\lambda}$ and $\overline{y_\lambda}$ from Eqs. (35) and (36), respectively.

This mapping of the PES onto the $\overline{x_\lambda}$, $\overline{y_\lambda}$ tangent plane is called the equatorial view because it corresponds to a nonperpendicular arclength preserving projection of the constant hyperradius hemisphere on a plane tangent to it at the point on its equator defined by $\omega_\lambda=\gamma_\lambda=\pi/2$. This permits the viewing of all three possible atom–diatom arrangement channels (for the triatomic reaction) as well as the regions for which the three atoms are at comparable distances from each

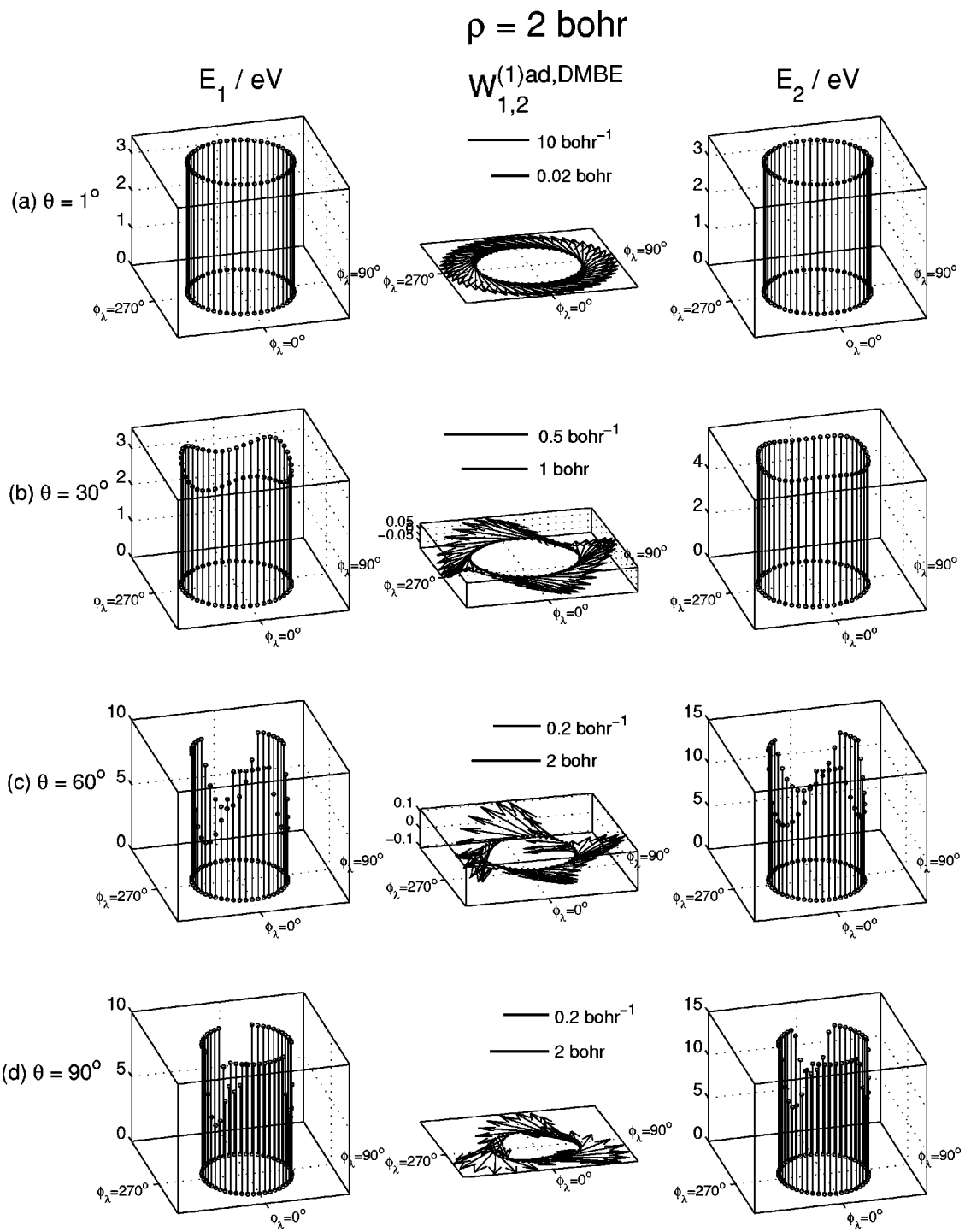

FIG. 8. DMBE nonadiabatic coupling vector, $\mathbf{W}_{1,2}^{(1)\mathrm{ad,DMBE}}$, ground state energy ($E_1$), and first-excited state energy (E_2) for $\rho=2$ bohr and (a) $\theta=1°$; (b) $\theta=30°$; (c) $\theta=60°$; (d) $\theta=90°$ (collinear). The scales have the same meaning as in Fig. 4.

other, for a fixed hyperradius ρ. Maps of this kind have been used before.[90,91,98]

In Figs. 1 and 2, we present the equatorial views for the lowest two PESs for H_3 obtained by the DSP and DMBE fits. The plots display the C_{3v} symmetry of the H_3 system. Also, the circle at the edge of each plot corresponds to collinear geometries ($\theta=\pi/2$) and the center of each plot corresponds to a conical intersection geometry ($\theta=0$). Figures 1(a) through 1(d) show the equatorial views of the equipotential contours of the $1\,^2A'$ surface for the DSP fit (E_1^{DSP}) to the *ab initio* data at constant values of the hyperradius ρ. Figures 1(e)–1(h) show the corresponding contours for the DMBE fit (E_1^{DMBE}). Figures 2(a)–2(h) show the corresponding equatorial views for the first-excited ($2\,^2A'$) surface. The DSP and DMBE fits are extremely similar for the ground PES ($1\,^2A'$), but show some differences in the first-excited PES ($2\,^2A'$).

For the ground PES ($1\,^2A'$) at $\rho=2$ bohr [Fig. 1(a)], there are no contours below 3.5 eV suggesting that at energies below 3.5 eV regions for which ρ is smaller than 2 bohr

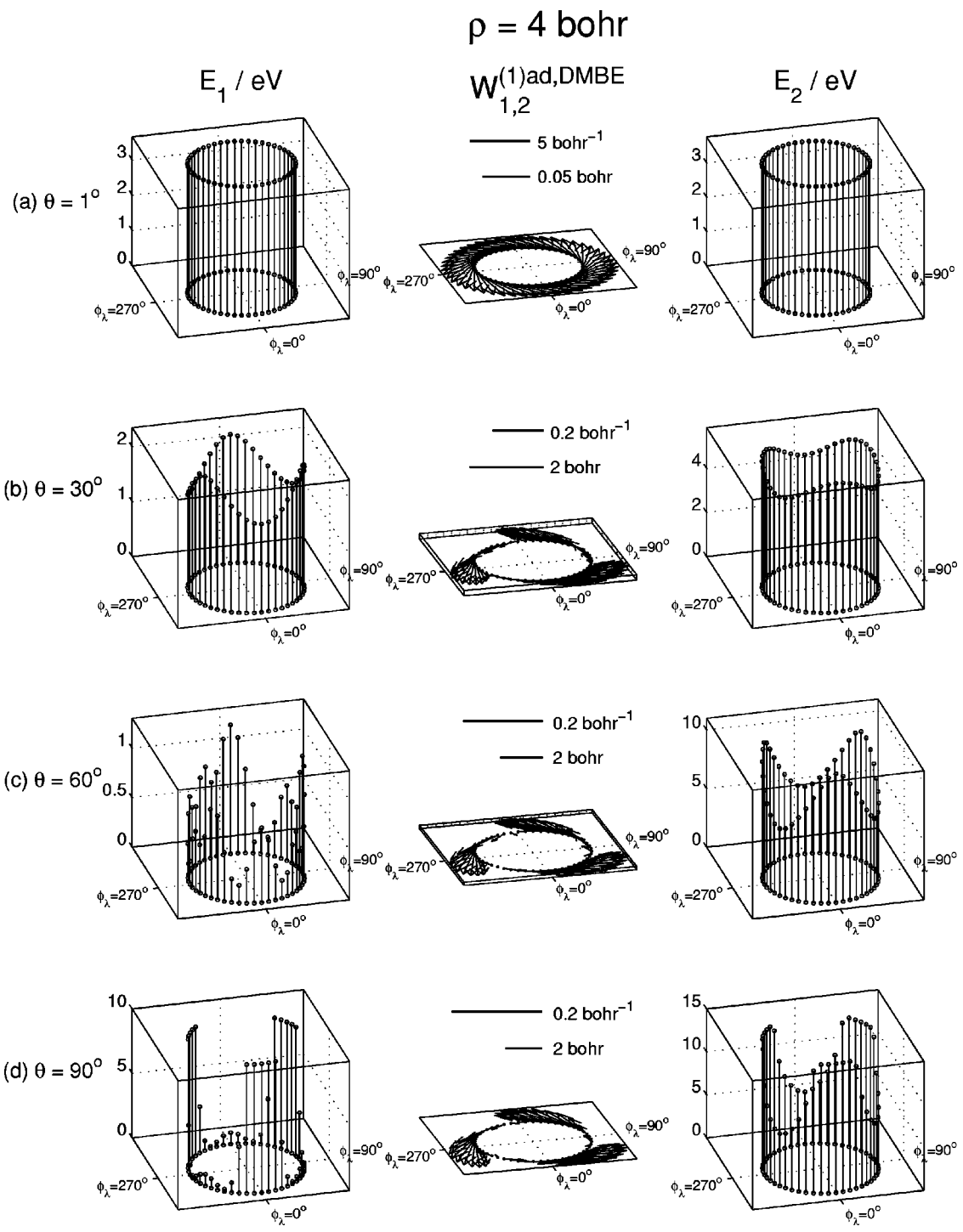

FIG. 9. Same as Fig. 8 for $\rho=4$ bohr.

will not be dynamically important. For all other ρ [Fig. 1(b)–1(d)], contours as low as 0.5 eV exist suggesting the dynamical importance of these higher ρ regions. In going from $\rho=4$ bohr [Fig. 1(b)] to $\rho=6$ bohr [Fig. 1(c)] to $\rho=8$ bohr [Fig. 1(d)], we are considering triatomic configurations whose overall size is increasing. For $\rho=4$ bohr the region near to the center of the figure corresponds to E_1 between 2.5 eV and a value less than 4.0 eV, whereas for $\rho=6$ bohr that energy lies between 4.0 eV and a value close to the dissociation limit of 4.75 eV and for $\rho=8$ bohr it is between 4.5 eV and that dissociation limit. This indicates that for large ρ and stretched configurations of the system, which those regions correspond to, the system approaches dissociation, as expected. The first-excited PES ($2\,^2A'$) is similar for both the DSP and DMBE PESs at $\rho=2$ bohr [Figs. 2(a) and 2(e)] and at $\rho=8$ bohr [Figs. 2(d) and 2(h)]. At $\rho=4$ bohr, the DSP PES [Fig. 2(b)] has a 6 eV contour that spreads over the entire surface, whereas this contour is closed for the DMBE PES [Fig. 2(f)]. On the other hand at $\rho=6$ bohr, the 5 eV contour spreads over the entire surface for the DMBE PES [Fig. 2(g)] but is closed for the DSP one [Fig. 2(b)].

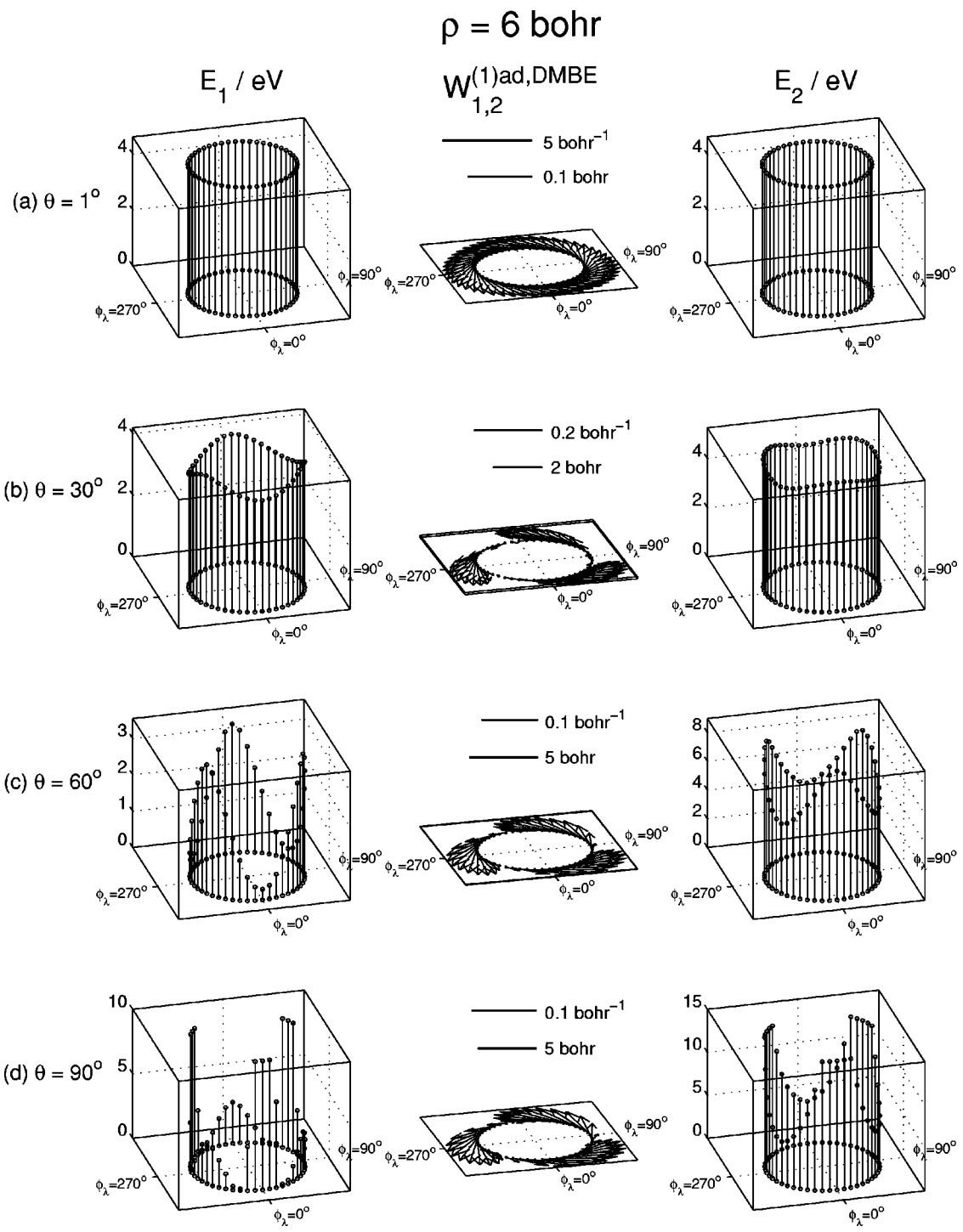

FIG. 10. Same as Fig. 8 for $\rho=6$ bohr.

For the ground PES, DSP fit (E_1^{DSP}) has a rms deviation of 1.15 kcal/mol relative to the Liu–Siegbahn–Truhlar–Horowitz (LSTH) PES[99] (E_1^{LSTH}) and of 1.03 kcal/mol relative to the DMBE one (E_1^{DMBE}) for energies below 5 eV. For the first-excited PES, DSP fit (E_2^{DSP}) has a rms deviation of 1.19 kcal/mol relative to the DMBE one (E_2^{DMBE}) for energies below 5 eV and of 2.97 kcal/mol for energies below 10 eV. E_1^{DSP} stays greater than E_1^{LSTH} and E_1^{DMBE} for most geometries (except for large geometries with ρ greater than 6 bohr near the conical intersection with θ smaller than 10°) in the internal nuclear configuration space, whereas E_2^{DSP} stays greater than E_2^{DMBE} only for compact geometries (ρ less than 4 bohr) near and slightly away from the conical intersection (θ less than 40°). This is due to the fact that *ab initio* electronic structure calculations were performed to obtain good representative ground and first-excited state energies used in the E_1^{DSP} and E_2^{DSP} fits. This leads to a slightly higher E_1^{DSP} than it would be if the basis set used was chosen to optimize the ground state energies only. Since E_2^{DMBE} PES is an ana-

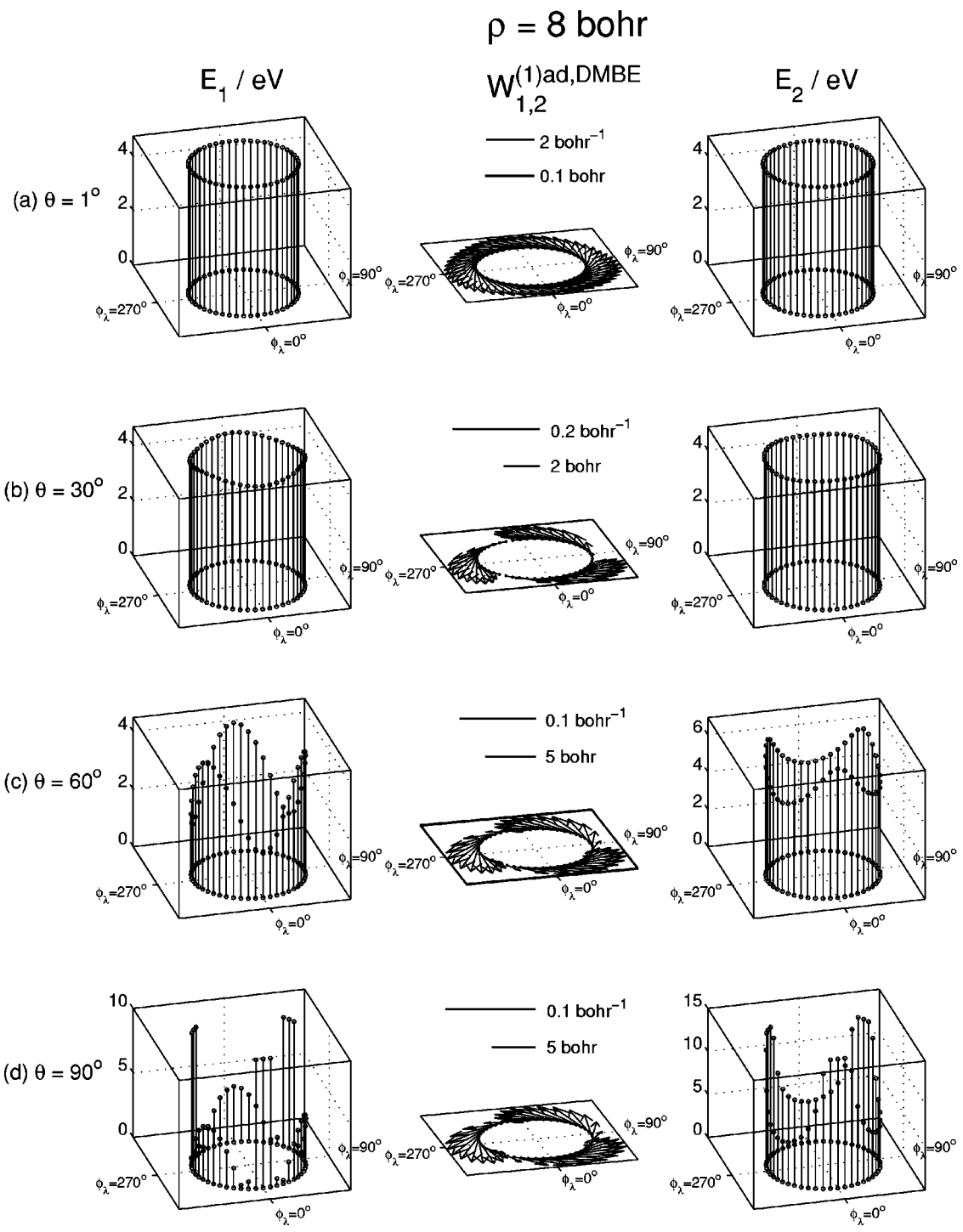

FIG. 11. Same as Fig. 8 for $\rho=8$ bohr.

lytic continuation of the E_1^{DMBE} PES, E_2^{DSP} PES is lower than E_2^{DMBE} for most nuclear geometries.

Overall, for the ground PES, the DMBE PES is accurate over the entire internal configuration space, but for the first-excited state PES, the similarities between DSP and DMBE PESs at $\rho=2$ and 8 bohr and the differences between them at $\rho=4$ and 6 bohr indicate that the DMBE PES is accurate in the compact and asymptotic regions, but not in the strong interaction regions.

IV. RESULTS AND DISCUSSION

A. *Ab initio* and DMBE first-derivative couplings

The first-derivative coupling vector $[\mathbf{W}_{1,2}^{(1)\mathrm{ad}}(\mathbf{q})]$ obtained using Eq. (8) had its three components defined in the ρ, θ, and ϕ_λ unit vector directions by Eqs. (9)–(11). These internal hyperpherical coordinates ($\mathbf{q}$: ρ, θ, ϕ_λ) defined in Sec. III B are identical to ordinary spherical polar coordinates except for the range of θ which is 0 to $\pi/2$ for the

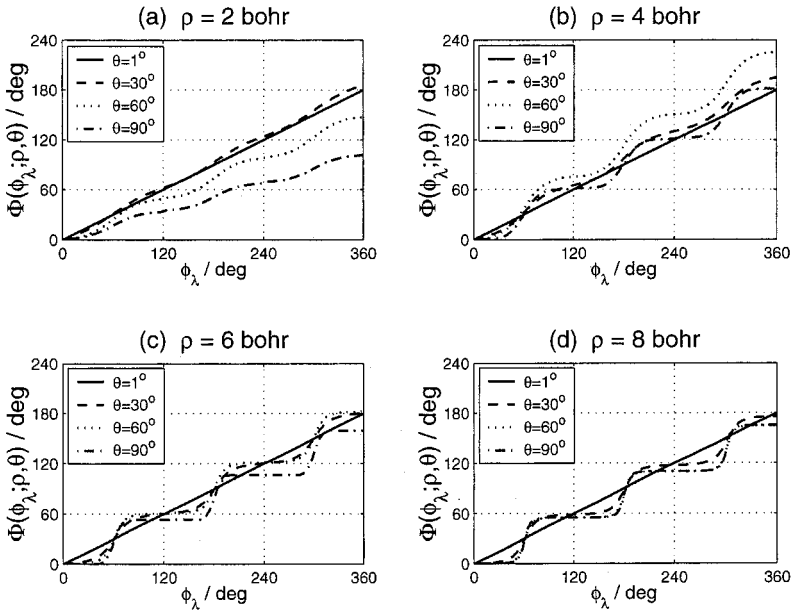

FIG. 12. Phase $\Phi(\phi_\lambda;\rho,\theta)$ as a function of ϕ_λ evaluated using Eq. (38) for four values of θ: 1° (solid line), 30° (dashed line), 60° (dotted line), and 90° (dash-dotted line) for each of the four values of ρ: (a) 2 bohr, (b) 4 bohr, (c) 6 bohr, and (d) 8 bohr.

former [Eq. (12)] compared to 0 to π for the latter. These internal hyperpherical coordinates span half a sphere (compared to the full sphere spanned by ordinary spherical polar coordinates). This property facilitates the visualization of the first-derivative coupling vector in the associated internal three-dimensional Cartesian coordinate configuration space. The transformation of this vector into its Cartesian counterpart, which has components $W^{(1)\mathrm{ad}}_{1,2,x}$, $W^{(1)\mathrm{ad}}_{1,2,y}$, and $W^{(1)\mathrm{ad}}_{1,2,z}$ in the *x*, *y*, and *z* unit vector directions defined as

$$\begin{pmatrix} W^{(1)\mathrm{ad}}_{1,2,x} \\ W^{(1)\mathrm{ad}}_{1,2,y} \\ W^{(1)\mathrm{ad}}_{1,2,z} \end{pmatrix} = \begin{pmatrix} \sin\theta\cos\phi_\lambda & \cos\theta\cos\phi_\lambda & -\sin\phi_\lambda \\ \sin\theta\sin\phi_\lambda & \cos\theta\sin\phi_\lambda & \cos\phi_\lambda \\ \cos\theta & -\sin\theta & 0 \end{pmatrix} \times \begin{pmatrix} W^{(1)\mathrm{ad}}_{1,2,\rho} \\ W^{(1)\mathrm{ad}}_{1,2,\theta} \\ W^{(1)\mathrm{ad}}_{1,2,\phi_\lambda} \end{pmatrix}. \tag{37}$$

In the central panels of Figs. 4–7, we present a perspective view of the three-dimensional *ab initio* first-derivative coupling vector at points in this space with varying values of the hyperangle ϕ_λ, for fixed values of the hyperradius ρ and hyperangle θ. In Cartesian language, this is equivalent to varying *x* and *y* and keeping *z* fixed, as indicated by the dotted horizontal circles in those figures. The Cartesian components of this vector were obtained from Eq. (37). The leftmost panels contain the corresponding DSP ground state electronic energies plotted as vertical lines such that the energies can be read off from the length of those vertical lines. The rightmost panels contain the DSP first-excited state electronic energies plotted in the same way as the ground state electronic energies. Figures 8–11 present the same physical quantities but obtained by the DMBE method. The Cartesian components of the longitudinal part of the DMBE first-derivative coupling vector are also obtained from Eq. (37). Figures 4, 5, 6, and 7 correspond to the fixed hyperradii of 2, 4, 6, and 8 bohr, respectively. The same is the case for Figs. 8, 9, 10, and 11. In all figures (4–11), panel (a) (the first row of plots) corresponds to $\theta=1°$ (a value very close to the conical intersection geometries of $\theta=0°$), panel (b) corresponds to $\theta=30°$, panel (c) to $\theta=60°$, and panel (d) to $\theta=90°$ (collinear geometries). The tail end of the vectors lie on a circle that corresponds to a fixed θ on the hemisphere in hyperspherical coordinate space defined by a fixed hyperradius ρ. This circle maps the full ϕ_λ range of 0°–360° and is shown on the bottom face of all E_1 and E_2 panels. The coupling vectors shown in the central panels correspond to the configurations being mapped by this circle. Above each of these central panels two scales are given. The one in units of bohr corresponds to the internal nuclear configuration space corresponding to the full 0°–360° ϕ_λ range spanned on the *xy* plane. The second one in units of bohr^{-1} corresponds to the three-dimensional space sampled by the *x*, *y*, and *z* components of the coupling vector. The two spaces coexist on the *xy* plane. In addition, in all figures the ground-state energies (E_1) have been cut off at 10 eV and the first-excited state electronic energies (E_2) at 15 eV.

The first-derivative coupling vector plots at $\theta=1°$ [panel (a) in Figs. 4–11] have been included to show their behavior near the conical intersection. The $\theta=90°$ [panel (d) in those figures] case has been included, as it corresponds to collinear geometries for the triatomic system. This case is important for lower energies due to the collinear dominance of the $H + H_2$ reaction at those energies, as will be discussed in Sec. IV C. The $\theta=30°$ and $\theta=60°$ cases [panels (b) and (c), respectively, in all figures] have been included to gauge the importance of the coupling vector away from the conical intersection as well as the collinear geometries.

For the DMBE case, the total first-derivative coupling vector $[\mathbf{W}^{(1)\mathrm{ad,DMBE}}_{1,2}(\mathbf{q})]$ is equal to its longitudinal part $[\mathbf{W}^{(1)\mathrm{ad,DMBE}}_{1,2,\mathrm{lon}}(\mathbf{q})]$ because the transverse part $[\mathbf{W}^{(1)\mathrm{ad,DMBE}}_{1,2,\mathrm{tra}}(\mathbf{q})]$ was neglected over the entire internal configuration space. Figures 8–11 show the DMBE's total (or

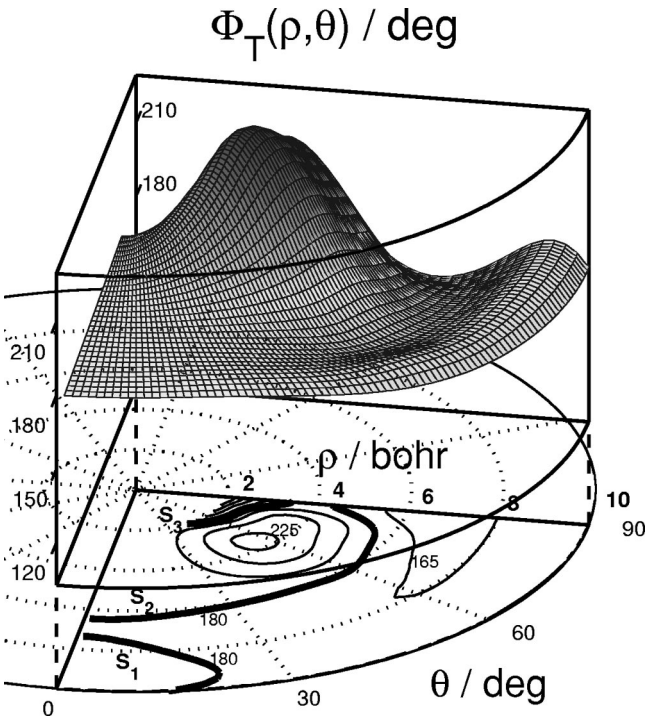

FIG. 13. Topological phase $\Phi_T(\rho,\theta)$ as a function of ρ and θ evaluated using Eq. (39). The contours on the bottom face correspond to $\Phi_T(\rho,\theta)$ values ranging from 150° to 225° every 15°. The three 180° contours have been shown in bold and labeled as $\mathbf{S}_1$, $\mathbf{S}_2$, and $\mathbf{S}_3$.

longitudinal) first-derivative coupling vector and the corresponding ground and first-excited DMBE energies for comparison with the *ab initio* first-derivative coupling vector plots. In Sec. IV C, the comparison between DMBE and *ab initio* first-derivative coupling vectors is discussed, based upon their magnitudes and the corresponding ground and first-excited energies. This discussion will help locate the regions of the internal hyperspherical configuration space for the $H+H_2$ reaction, for which the first-derivative couplings may affect the dynamics of that reaction.

B. The topological phase

In Sec. II A we mentioned how we can get some qualitative indication of possible non-negligible derivative couplings between the $2\,^2A'$ and $3\,^2A'$ PESs of H_3. This involves calculating the topological phase $\Phi_T(\mathcal{L})$ from Eq. (17) along closed loops around the conical intersection between the $1\,^2A'$ and $2\,^2A'$ states. A nonzero $\eta(\mathcal{L})$ [defined by Eq. (18)] is indicative of such non-negligible couplings (see Sec. II A).

In our symmetrized hyperspherical coordinates, **q** is a set of the three coordinates ρ, θ, and ϕ_λ. The above-mentioned original conical intersection between the $1\,^2A'$ and $2\,^2A'$ states lies along $\theta=0°$ for all values of ρ. ϕ_λ is undefined at $\theta=0°$. To evaluate the integral in Eq. (16) along an open loop around that conical intersection, we take a circular path $\mathcal{L}$ given by a fixed value of $\theta\neq 0°$, a fixed ρ, and ϕ_λ varying along that path from 0 to an arbitrary value, according to

$$\Phi(\phi_\lambda,0;\rho,\theta)=\int_0^{\phi_\lambda} W^{(1)\mathrm{ad}}_{1,2,\phi_\lambda}(\rho,\theta,\phi'_\lambda)\rho\sin\theta\, d\phi'_\lambda, \quad (38)$$

where $W^{(1)\mathrm{ad}}_{1,2,\phi_\lambda}(\rho,\theta,\phi'_\lambda)$ is defined in Eq. (11). These integrals are evaluated using the standard Simpson numerical integration quadrature. From here on, we will drop the 0 in $\Phi(\phi_\lambda,0;\rho,\theta)$ and just refer to it as $\Phi(\phi_\lambda;\rho,\theta)$.

In Fig. 12 we show the open path phase $\Phi(\phi_\lambda;\rho,\theta)$ as a function of ϕ_λ evaluated using Eq. (38) for four values of ρ (2, 4, 6, and 8 bohr) and four values of θ (1°, 30°, 60°, and 90°). For each ρ and θ we then calculate the closed-loop integral (or the topological phase) Φ_T. This corresponds to a complete loop around the conical intersection [$\phi_\lambda=2\pi$ in Eq. (38)] and is expressed as

$$\Phi_T(\rho,\theta)=\oint W^{(1)\mathrm{ad}}_{1,2,\phi_\lambda}(\rho,\theta,\phi'_\lambda)\rho\sin\theta d\phi'_\lambda. \quad (39)$$

In Fig. 13 we display this topological phase as a function of ρ and θ for the entire (ρ,θ) space considered in this paper.

C. Discussion

As mentioned in Sec. IV A, Figs. 4–7 display the *ab initio* first-derivative coupling vector and the corresponding DSP ground and first-excited electronic state energies for $\rho=2$ through 8 bohr, in steps of 2 bohr. Each of the figures has four sets of panels: (a) $\theta=1°$ (triatomic geometries near conical intersection), (b) $\theta=30°$, (c) $\theta=60°$, and (d) $\theta=90°$ (collinear triatomic geometries).

Figure 4(a) ($\rho=2$ bohr and $\theta=1°$) corresponds to a very compact set of geometries near the conical intersection. Being near the conical intersection (where the two electronic states are degenerate), the ground (E_1) and the first-excited (E_2) state energies are close to each other and stay around 3.3 eV as a function of ϕ_λ. The first-derivative coupling vector has a large magnitude (between 10 and 15 bohr^{-1}) but its z component is very small compared to its length, due to a singularity at the conical intersection geometries. This dominance of the x and y components translates into a strong dominance of the ϕ_λ component of the first-derivative coupling vector near the conical intersection. Figure 4(b) (ρ

TABLE III. Range of the largest and smallest internuclear distances and largest bond angle over the full 0 to 2π range of ϕ_λ.

		$\rho=2$ bohr		$\rho=4$ bohr		$\rho=6$ bohr		$\rho=8$ bohr	
θ	$\gamma_\lambda^{\max}$	$R_{\lambda\nu}^{\min}$	$R_{\lambda\nu}^{\max}$	$R_{\lambda\nu}^{\min}$	$R_{\lambda\nu}^{\max}$	$R_{\lambda\nu}^{\min}$	$R_{\lambda\nu}^{\max}$	$R_{\lambda\nu}^{\min}$	$R_{\lambda\nu}^{\max}$
1°	90.5–91.0°	1.50–1.51	1.52–1.53	3.01–3.03	3.05–3.07	4.52–4.54	4.58–4.60	6.03–6.05	6.11–6.13
30°	106.1–120.0°	1.07–1.32	1.70–1.86	2.15–2.63	3.40–3.72	3.22–3.95	5.10–5.58	4.30–5.26	6.80–7.44
60°	130.9–150.0°	0.56–1.14	1.82–2.08	1.11–2.29	3.64–4.15	1.67–3.43	5.46–6.23	2.23–4.58	7.28–8.30
90°	180.0–180.0°	0.00–1.07	1.86–2.15	0.00–2.15	3.72–4.30	0.00–3.22	5.58–6.45	0.00–4.30	7.44–8.60

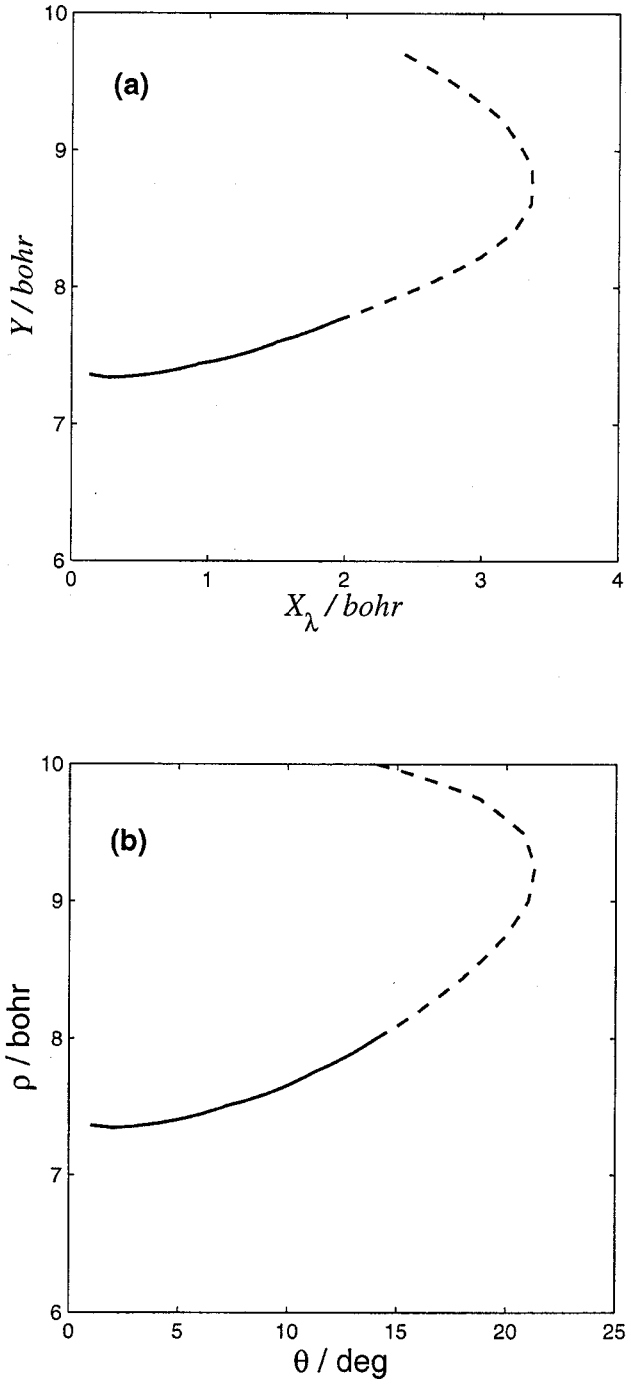

FIG. 14. (a) The 180° $\mathbf{S}_1$ contour of Fig. 13 shown in the $X_\lambda Y$ plane of Fig. 3. (b) The same contour shown in the regular (ρ,θ) plane. (The dashed points correspond to values of ρ greater than 8 bohr.)

$=2$ bohr and $\theta=30°$) corresponds to a compact set of geometries further away from the conical intersection (but with the largest bond angle in the range 106°–120° and the smallest bond length around 1.5 bohr, as seen in Table III). This manifests itself in the fact that for this θ the E_1 and E_2 energies are quite different from each other, the former staying above 3.1 eV and varying slowly between 3.1 and 3.5 eV as a function of ϕ_λ with the latter staying around 6 eV and varying even more slowly with ϕ_λ. The coupling vector is smaller in magnitude (with a maximum around 1 bohr^{-1} and an average around 0.5 bohr^{-1}) than for Fig. 4(a) due to its greater distance from the conical intersection configurations.

Figure 4(c) ($\rho=2$ bohr and $\theta=60°$) corresponds to compact geometries (with the largest bond angle in the range 140°–150° and the smallest bond length in the range 0.56–1.14 bohr, as seen in Table III) even further removed from the conical intersection. The E_1 and E_2 energies are again quite different from each other, and vary more rapidly with ϕ_λ than before [Fig. 4(b)]. The E_1 energies vary between 4 eV and some value higher than 10 eV as a function of ϕ_λ, while the E_2 energies vary between 7 eV and some value higher than 15 eV with ϕ_λ. Both E_1 and E_2 display maxima at $\phi_\lambda=0°$, 120°, and 240°. The coupling vector is again smaller in magnitude (with a maximum around 0.5 bohr^{-1} and averaging around 0.3 bohr^{-1}) than for $\theta=1°$ [Fig. 4(a)] but varies more rapidly with ϕ_λ as compared to the $\theta=30°$ case [Fig. 4(b)]. The *x*, *y*, and *z* components are comparable with each other contrary to the $\theta=1°$ [Fig. 4(a)] and $\theta=30°$ [Fig. 4(b)] cases. Figure 4(d) ($\rho=2$ bohr and $\theta=90°$) corresponds to compact collinear geometries with the smallest bond length in the range 0–1 bohr. The E_1 and E_2 energies are again quite different from each other, and vary even more rapidly with ϕ_λ than before [Fig. 4(c)] with minima around 5 and 8 eV, respectively. Both E_1 and E_2 have maxima at $\phi_\lambda=0°$, 120°, and 240° as for the $\theta=30°$ case [Fig. 4(c)], as at these configurations two out of three atoms are superimposed on each other. The coupling vector is small (averaging around 0.5 bohr^{-1}) as compared to the $\theta=1°$ case [Fig. 4(a)], and has a negligible *z* component compared to the $\theta=30°$ [Fig. 4(b)] and $\theta=60°$ [Fig. 4(c)] cases. Both E_1 and E_2 energies over the entire $\rho=2$ bohr configuration (compact geometries) space are 3.1 eV or higher and are expected to be of dynamical importance only at energies slightly below that value or higher.

Figure 5 presents the first-derivative coupling vector and the E_1 and E_2 energies for $\rho=4$ bohr. This hyperradius is of dynamical importance for energies significantly below the lowest conical intersection energy of 2.75 eV (which occurs at $\rho_{\text{min}}\equiv 2.6$ bohr for the DMBE PES[54]), and is also expected to be of importance at that energy and above since the conical intersection energy increases rather slowly with ρ above ρ_{min}. The $\theta=1°$ case [Fig. 5(a)] is similar to the one for $\rho=2$ bohr [Fig. 4(a)]. E_1 and E_2 are close to each other and are approximately equal to 3.6 eV. The coupling vector has large *x* and *y* components (10 bohr^{-1}) and a negligible *z* component, again translating into a strong dominance of its ϕ_λ component near the conical intersection. At $\theta=30°$ [Fig. 5(b)], E_1 is as low as 1.5 eV, E_2 is 5 eV or larger, and the coupling vector has a smaller magnitude than for $\theta=1°$ [Fig. 5(a)]. At $\theta=60°$ [Fig. 5(c)], E_1 is as small as 0.25 eV, E_2 is 6 eV or larger, and the coupling vector has about the same magnitude as that at $\theta=30°$ [Fig. 5(b)]. At $\theta=90°$ [Fig. 5(d)], which corresponds to collinear geometries, E_1 can be as low as 0.2 eV and varies rapidly with ϕ_λ than for smaller values of θ and E_2 is again 6 eV or larger. The coupling vector has a larger *z* component than for the lower values of θ discussed. Collinear geometries are important for low collision energies.[47] Their importance at energies close to and above conical intersection energies is likely to be signifi-

cantly smaller or perhaps negligible but this remains to be determined by future scattering calculations.

For the $\rho=6$ bohr (Fig. 6) and 8 bohr (Fig. 7) cases, which correspond to triatomic large sized geometries (see Table III), the electronic energies are fairly similar to the $\rho=4$ bohr case (Fig. 5). In both these cases, E_1 can be as low as 0.2 eV. The coupling vector magnitudes on the other hand are smaller on average and have sharper maxima compared to the $\rho=4$ bohr case at around $\phi_\lambda=60°$, 180°, and 300°. They all have negligible z components, but their maxima occur in low energy regions. The coupling vectors presented in Figs. 6 and 7 may also affect the dynamics of the $H+H_2$ reaction depending on their magnitudes.

A similar detailed analysis of the DMBE first-derivative coupling vectors (Figs. 8–11) leads to the following conclusions. For $\rho=2$ bohr (Fig. 8), the coupling vector has a z component which is negligible in the vicinity of the conical intersection ($\theta=1°$) and at the collinear geometries ($\theta=90°$) but non-negligible in the intermediate regions. For all other values of the hyperradii ($\rho=4$, 6, and 8 bohr), that z component is negligible over the entire θ,ϕ_λ space (Figs. 9–11), which indicates the dominance of the ϕ_λ component. This stems from the fact that the DMBE coupling vector is purely longitudinal and given by Eqs. (19) and (20). A comparison of the DMBE first-derivative coupling vectors with the corresponding *ab initio* couplings confirms the previously stated fact that the DMBE's coupling vector has the right physical and quantitative behavior in the vicinity of the conical intersection. The differences between these two vectors, which occur even at low energies, stem mainly from the fact that the *ab initio* couplings include both a longitudinal part and a transverse part, whereas the DMBE couplings only include a longitudinal part, which is a good approximation to the *ab initio* longitudinal part in the vicinity of a conical intersection.

Figure 12 shows the open path phase $\Phi(\phi_\lambda;\rho,\theta)$ for four values of θ (1°, 30°, 60°, and 90°) and four values of ρ [(a) 2 bohr, (b) 4 bohr, (c) 6 bohr, and (d) 8 bohr] as a function of ϕ_λ as defined by Eq. (38). It shows how the open path phase Φ increases with ϕ_λ along a loop around the conical intersection between the $1\,^2A'$ and $2\,^2A'$ electronic states. For the $\theta=1°$ case (solid line in all four panels), to a very good approximation (0.2% or smaller difference) Φ is equal to $\phi_\lambda/2$ for all values of ρ considered. This is clearly expected because $\theta=1°$ is a region very close to the conical intersection and the $\phi_\lambda/2$ is a leading term of the diabatization angle in that region. For other values of θ, Φ fluctuates around some mean value proportional to ϕ_λ. The deviation of this mean value from $\phi_\lambda/2$ is dependent both on ρ and θ. Also, Φ returns to its mean value at regular intervals of 60° in ϕ_λ. As a result, we can approximate Φ by a sum of two terms, the first one being proportional to ϕ_λ and the second more complicated one possessing the C_{3v} symmetry (of H_3) via a $\sin 3\phi_\lambda$ dependence. The fluctuations in Φ about the mean value arise only from this second term and have an amplitude which increases monotonically with ρ between $\rho=2$ bohr and $\rho=8$ bohr. This seems to stem from the fact that for a large value of ρ, the length of the circular loop around the conical intersection is large, which leads to a large phase accumulation in these fluctuations.

Figure 13 shows the topological phase $\Phi_T(\rho,\theta)$ [defined by Eq. (39)] as a function of ρ and θ over the ρ space of 2–10 bohr and the θ space of 1°–90°. $\Phi_T=180°$ values correspond to a purely longitudinal first-derivative coupling vector. Any deviation of $\Phi_T(\rho,\theta)$ from this value suggests a nonzero transverse (*nonremovable*) part of the coupling vector.[42,61] On the bottom part of Fig. 13 we show contours corresponding to fixed values of $\Phi_T(\rho,\theta)$ ranging from 150° to 225° every 15°. The 180° contour has been shown in bold lines and its different segments labeled $\mathbf{S}_1$, $\mathbf{S}_2$, and $\mathbf{S}_3$. For small values of θ and all ρ, the values of $\Phi_T(\rho,\theta)$ stay reasonably constant and equal to 180°. This is expected because these small values of θ correspond to regions near the conical intersection, where the transverse component of the first-derivative coupling vector is expected to be negligible. This flat portion of the Φ_T surface is quite narrow at small ρ and gets wider as ρ increases. Also, for small values of ρ (<6 bohr) $\Phi_T(\rho,\theta)$ first increases and then drops as a function of θ. Beyond $\rho=6$ bohr, $\Phi_T(\rho,\theta)$ first drops somewhat and then increases slightly to a value under 180° as a function of θ.

The phase $\Phi_T(\rho,\theta)$ plotted in Fig. 13 gives an indication of the presence of non-negligible derivative couplings in the regions of (ρ,θ) space where it is different from 180°. In the present work, we have computed this phase over the entire dynamically important part of configuration space. In the absence of additional electronic state calculations, no method exists, to the best of our knowledge, that quantitatively correlates the deviation of this phase from 180° (over the whole configuration space) with the non-negligible derivative couplings that arise from nonadiabatic interactions involving states outside the two-adiabatic-state space. The 180° contour segments $\mathbf{S}_2$ and $\mathbf{S}_3$ in Fig. 13 are embedded in regions of (ρ,θ) configuration space, where $\Phi_T(\rho,\theta)$ deviates substantially from 180° and hence are not expected to contain information about any glancing interaction or conical intersections between the $2\,^2A'$ and $3\,^2A'$ states of H_3. Such is not the case for the $\mathbf{S}_1$ segment. In Fig. 14, we display this segment in two representations. Figure 14(a) shows it in the $X_\lambda Y$ plane of Fig. 3 and Fig. 14(b) in the regular $\rho-\theta$ plane. The points corresponding to ρ greater than 8 bohr have been indicated as dashed lines because they are a result of an extrapolation of the computed couplings and hence should not be used to draw any conclusions. Points below the solid curves correspond to extended regions of configuration space for which $\Phi_T(\rho,\theta)$ deviates from 180° and indicates that the value of $\mathbf{W}^{(1)\mathrm{ad}}_{1,2,\mathrm{tra}}$ is non-negligible in those regions. These solid curves seem to suggest the presence of intersection lines or avoided intersections between the $2\,^2A'$ and $3\,^2A'$ PESs in the $(\rho,\theta,\phi_\lambda)$ space, where ϕ_λ might correspond to three possible sets of C_{2v} configurations. It can either be the (0°,120°,240°) set or the (60°,180°,300°) set, or even both. A possible conical intersection between the $2\,^2A'$ and $3\,^2A'$ states was suggested by Yarkony[42] earlier for H_3. An alternate explanation may be that, at the values of ρ of relevance to Fig. 14, the curl of $\mathbf{W}^{(1)\mathrm{ad}}_{1,2}$ (or, equivalently, of its transverse part) is large.[100]

Calculations of the energy of the $3\,^2A'$ state of H_3 and of its first-derivative couplings with the $2\,^2A'$ state are needed to help establish a quantitative correlation between possible conical intersections involving those two states and the topological phase between the $1\,^2A'$ and $2\,^2A'$ states. The regions of nuclear configuration space, where the effect of nonadiabatic couplings (between the $2\,^2A'$ and $3\,^2A'$ states) is being felt, have many low energy regions, suggesting that the *nonremovable* part of the nonadiabatic couplings (between the $1\,^2A'$ and $2\,^2A'$ states) cannot be ignored and may play a significant role in the dynamics of the $H+H_2$ reaction, due to its presence in the diabatic nuclear motion Schrödinger equation.[12]

V. SUMMARY AND CONCLUSIONS

We have presented the results of accurate calculations of the first-derivative coupling vector between the $1\,^2A'$ and $2\,^2A'$ states of the H_3 system. These calculations were performed over the entire internal nuclear configuration space of this system of possible importance for its reactive scattering, up to total energies of about 5 eV. In addition, a fit (DSP) to its ground and first-excited electronic energies obtained by *ab initio* methods is given. The couplings are found to be nonnegligible even away from the conical intersection between these states, and can be used to obtain their longitudinal (removable) and transverse (nonremovable) parts. We have also compared our results with the DMBE ones,[54] which have built into them the right physical behavior in the vicinity of the conical intersection geometries. The DMBE ground-state electronic energies agree well with the DSP fit to the *ab initio* energies, while the first-excited ones show some significant differences. The DMBE couplings are purely longitudinal and hence fully *removable* upon an adiabatic to diabatic transformation. They compare well with the *ab initio* ones only in the neighborhood of the conical intersection, as expected.

We have also investigated the line integrals (along closed paths around the conical intersection between these electronic states) of the *ab initio* couplings over the entire nuclear configuration space considered. We found large deviations of the topological phase $\Phi_T(\rho,\theta)$ from π suggesting the existence of conical intersections between the $2\,^2A'$ and $3\,^2A'$ states and/or the presence of non-negligible derivative couplings involving excluded electronic states. Electronic energy calculations for the $3\,^2A'$ state and its first-derivative couplings with the $2\,^2A'$ state could lead to a quantitative correlation between the topological phase between the $1\,^2A'$ and $2\,^2A'$ states and the locus of possible intersection geometries between the $2\,^2A'$ and $3\,^2A'$ states.

ACKNOWLEDGMENTS

This work has been supported in part by NSF Grant Nos. CHE 9810050 (A.K.) and CHE 9700771 (D.R.Y.).

[1] G. Nyman and H.-G. Yu, Rep. Prog. Phys. **63**, 1001 (2000).
[2] *Dynamics of Molecules and Chemical Reactions*, edited by R. E. Wyatt and J. Z. H. Zhang (Dekker, New York, 1996).
[3] *Theory of Chemical Reaction Dynamics*, edited by M. Baer (CRC, Boca Raton, 1985), Vols. I and II.
[4] J. Z. H. Zhang, J. Q. Dai, and W. Zhu, J. Phys. Chem. A **101**, 2746 (1997).
[5] S. K. Pogrebnya, J. Palma, D. C. Clary, and J. Echave, Phys. Chem. Chem. Phys. **2**, 693 (2000).
[6] G. Herzberg and H. C. Longuet-Higgins, Discuss. Faraday Soc. **35**, 77 (1963).
[7] H. C. Longuet-Higgins, Proc. R. Soc. London, Ser. A **344**, 147 (1975).
[8] H. C. Longuet-Higgins, Adv. Spectrosc. (N.Y.) **2**, 429 (1961).
[9] C. A. Mead and D. G. Truhlar, J. Chem. Phys. **70**, 2284 (1979).
[10] C. A. Mead, Chem. Phys. **49**, 23 (1980).
[11] M. V. Berry, Proc. R. Soc. London, Ser. A **392**, 45 (1984).
[12] A. Kupperman, in Ref. 2, pp. 411–472.
[13] Y. Aharonov and D. Bohm, Phys. Rev. **115**, 485 (1969).
[14] Y.-S. M. Wu, A. Kuppermann, and B. Lepetit, Chem. Phys. Lett. **186**, 319 (1991).
[15] Y.-S. M. Wu and A. Kuppermann, Chem. Phys. Lett. **201**, 178 (1993).
[16] A. Kuppermann and Y.-S. M. Wu, Chem. Phys. Lett. **205**, 577 (1993).
[17] Y.-S. M. Wu and A. Kuppermann, Chem. Phys. Lett. **235**, 105 (1995).
[18] A. Kuppermann and Y.-S. M. Wu, Chem. Phys. Lett. **241**, 229 (1995).
[19] D. A. V. Kliner, K. D. Rinen, and R. N. Zare, Chem. Phys. Lett. **166**, 107 (1990).
[20] D. A. V. Kliner, D. E. Adelman, and R. N. Zare, J. Chem. Phys. **95**, 1648 (1991).
[21] D. Neuhauser, R. S. Judson, D. J. Kouri, D. E. Adelman, N. E. Shafer, and D. A. V. Kliner, Science **257**, 519 (1992).
[22] D. E. Adelman, N. E. Shafer, D. A. V. Kliner, and R. N. Zare, J. Chem. Phys. **97**, 7323 (1992).
[23] M. Born, Nachr. Akad. Wiss. Gött. Math.-Phys. Kl. Article No. 6, 1 (1951).
[24] M. Born and K. Huang, *Dynamical Theory of Crystal Lattice* (Oxford University Press, Oxford, 1954), pp. 166–177 and 402–407.
[25] R. J. Buenker, G. Hirsch, S. D. Peyerimhoff, P. J. Bruna, J. Römelt, M. Bettendorff, and C. Petrongolo, in *Current Aspects of Quantum Chemistry* (Elsevier, New York, 1981), pp. 81–97.
[26] M. Desouter-Lecomte, C. Galloy, J. C. Lorquet, and M. V. Pires, J. Chem. Phys. **71**, 3661 (1979).
[27] B. H. Lengsfield, P. Saxe, and D. R. Yarkony, J. Chem. Phys. **81**, 4549 (1984).
[28] P. Saxe, B. H. Lengsfield, and D. R. Yarkony, Chem. Phys. Lett. **113**, 159 (1985).
[29] B. H. Lengsfield and D. R. Yarkony, J. Chem. Phys. **84**, 348 (1986).
[30] J. O. Jensen and D. R. Yarkony, J. Chem. Phys. **89**, 975 (1988).
[31] V. Sidis, in *State-selected and State-to-State Ion- Molecule Reaction Dynamics Part 2, Theory, Vol. 82*, edited by M. Baer and C.-Y. Ng (Wiley, New York, 1992), pp. 73–134.
[32] M. Baer, Chem. Phys. Lett. **35**, 112 (1975).
[33] C. A. Mead and D. G. Truhlar, J. Chem. Phys. **77**, 6090 (1982).
[34] C. A. Mead, J. Chem. Phys. **78**, 807 (1983).
[35] T. Pacher, L. S. Cederbaum, and H. Köppel, J. Chem. Phys. **89**, 7367 (1988).
[36] E. Mercier and G. Chambaud, J. Phys. B **20**, 4659 (1987).
[37] T. Pacher, C. A. Mead, L. S. Cederbaum, and H. Köppel, J. Chem. Phys. **91**, 7057 (1989).
[38] T. Pacher, H. Köppel, and L. S. Cederbaum, J. Chem. Phys. **95**, 6668 (1991).
[39] M. Baer and R. Englman, Mol. Phys. **75**, 293 (1992).
[40] I. D. Petasalakis, G. Theodorakopoulos, and C. A. Nicolaides, J. Chem. Phys. **97**, 7623 (1992).
[41] K. Ruedenberg and G. J. Atchity, J. Chem. Phys. **99**, 3799 (1993).
[42] D. R. Yarkony, J. Chem. Phys. **105**, 10456 (1996).
[43] R. Thurwachter and P. Halvick, Chem. Phys. **221**, 33 (1997).
[44] V. M. Garcia, M. Reguero, R. Caballol, and J. P. Malrieu, Chem. Phys. Lett. **281**, 161 (1997).
[45] H. Nobutoki, Int. J. Quantum Chem. **74**, 745 (1999).
[46] D. R. Yarkony, J. Chem. Phys. **114**, 2601 (2001).
[47] G. C. Schatz and A. Kuppermann, J. Chem. Phys. **65**, 4668 (1976).
[48] W. H. Miller and J. Z. H. Zhang, J. Phys. Chem. **95**, 12 (1991).
[49] R. T. Pack and G. A. Parker, J. Chem. Phys. **87**, 3888 (1987).
[50] F. Webster and J. C. Light, J. Chem. Phys. **90**, 300 (1989).
[51] C. A. Mead, J. Chem. Phys. **72**, 3839 (1980).

[52] B. Lepetit and A. Kuppermann, Chem. Phys. Lett. **166**, 581 (1990).
[53] Z. Peng, Ph.D. thesis, California Institute of Technology, Pasadena, CA (1991).
[54] A. J. C. Varandas, F. B. Brown, C. A. Mead, D. G. Truhlar, and N. C. Blais, J. Chem. Phys. **86**, 6258 (1987).
[55] B. H. Lengsfield and D. R. Yarkony, in *State-selected and State to State Ion-Molecule Reaction Dynamics: Part 2 Theory, Vol. 82,* edited by M. Baer and C.-Y. Ng (Wiley, New York, 1992), pp. 1–71.
[56] C. Galloy and J. C. Lorquet, J. Chem. Phys. **67**, 4672 (1971).
[57] H. J. Werner and W. Meyer, J. Chem. Phys. **74**, 5802 (1981).
[58] D. Dehareng, X. Chapuisat, J. C. Lorquet, C. Galloy, and G. Raseev, J. Chem. Phys. **78**, 1246 (1983).
[59] H. J. Werner, B. Follmeg, and M. H. Alexander, J. Chem. Phys. **89**, 3139 (1988).
[60] D. R. Yarkony, J. Phys. Chem. A **101**, 4263 (1997).
[61] N. Matsunaga and D. R. Yarkony, J. Chem. Phys. **107**, 7825 (1997).
[62] N. Matsunaga and D. R. Yarkony, Mol. Phys. **93**, 79 (1998).
[63] D. R. Yarkony, Mol. Phys. **93**, 971 (1998).
[64] D. R. Yarkony, J. Chem. Phys. **84**, 3206 (1986).
[65] J. O. Jensen and D. R. Yarkony, J. Chem. Phys. **90**, 1657 (1989).
[66] H. J. Silverstone and O. Sinanoglu, J. Chem. Phys. **44**, 1899 (1966).
[67] I. Shavitt, *Modern Theoretical Chemistry* (Plenum, New York, 1976), Vol. 3.
[68] H. J. Werner, in *Advances in Chemical Physics*, edited by K. P. Lawley (Wiley, New York, 1987), Vol. 69, p. 1.
[69] B. O. Roos, P. R. Taylor, and P. E. M. Siegbahn, Chem. Phys. **48**, 157 (1980).
[70] B. O. Roos, Int. J. Quantum Chem., Quantum Chem. Symp. **14**, 175 (1980).
[71] P. Siegbahn, A. Heiberg, B. Roos, and B. Levy, Phys. Scr. **21**, 323 (1980).
[72] H. J. Werner and W. Meyer, J. Chem. Phys. **74**, 5794 (1981).
[73] B. H. Lengsfield, J. Chem. Phys. **77**, 4073 (1982).
[74] W. H. Press, S. A. Teukolsky, W. T. Vetterling, and B. P. Flannery, *Numerical Recipes in Fortran: The Art of Scientific Computing* (Cambridge University Press, Cambridge, 1992), pp. 116–122.
[75] P. M. Morse and H. Feshbach, *Methods of Theoretical Physics* (McGraw–Hill, New York, 1953), pp. 52–54, 1763.
[76] R. G. Sadygov and R. D. Yarkony, J. Chem. Phys. **109**, 20 (1998).
[77] M. Baer, Chem. Phys. **15**, 49 (1976).
[78] R. Englman, A. Yahalom, and M. Baer, Eur. Phys. J. D **8**, 1 (2000).
[79] R. Englman and M. Baer, J. Phys.: Condens. Matter **11**, 1059 (1999).
[80] A. M. Mebel, M. Baer, V. M. Rozenbaum, and S. H. Lin, Chem. Phys. Lett. **336**, 135 (2001).
[81] B. Liu, J. Chem. Phys. **58**, 1925 (1973).
[82] P. Siegbahn and B. Liu, J. Chem. Phys. **68**, 2457 (1978).
[83] M. R. A. Blomberg and B. Liu, J. Chem. Phys. **82**, 1050 (1985).
[84] R. N. Porter, R. M. Stevens, and M. Karplus, J. Chem. Phys. **49**, 5163 (1968).
[85] T. C. Thompson and C. A. Mead, J. Chem. Phys. **82**, 2408 (1985).
[86] T. C. Thompson, G. Izmirlian, Jr., S. J. Lemon, D. G. Truhlar, and C. A. Mead, J. Chem. Phys. **82**, 5597 (1985).
[87] K. D. Jordan, Chem. Phys. **9**, 199 (1975).
[88] T. Ho and H. Rabitz, J. Chem. Phys. **104**, 2584 (1996).
[89] A. Frishman, D. K. Hoffman, and D. J. Kouri, J. Chem. Phys. **107**, 804 (1997).
[90] S. Rogers, D. Wang, S. Walch, and A. Kuppermann, J. Phys. Chem. A **104**, 2308 (2000).
[91] A. Kuppermann, Chem. Phys. Lett. **32**, 374 (1975).
[92] L. M. Delves, Nucl. Phys. **9**, 391 (1959).
[93] L. M. Delves, Nucl. Phys. **20**, 275 (1960).
[94] D. Jepsen and J. O. Hirschfelder, Proc. Natl. Acad. Sci. U.S.A. **45**, 249 (1959).
[95] F. T. Smith, J. Math. Phys. **3**, 735 (1962).
[96] A. Kuppermann, in *Advances in Molecular Vibrations and Collision Dynamics*, edited by J. Bowman (JAI, Greenwich, CT, 1994), Vol. 2B, pp. 117–186.
[97] R. T. Ling and A. Kuppermann, in *Electronic and Atomic Collisions, Abstract of the 9th International Conference on the Physics of Electronic and Atomic Collisions, Seattle, Washington, 24–30 July 1975*, edited by J. S. Riley and R. Geballe (University of Washington Press, Seattle, 1975), Vol. 1, pp. 353–354.
[98] Y.-S. M. Wu, A. Kuppermann, and J. B. Anderson, Phys. Chem. Chem. Phys. **6**, 929 (1999).
[99] D. G. Truhlar and C. J. Horowitz, J. Chem. Phys. **68**, 2466 (1978); **71**, 1514(E) (1979).
[100] R. G. Sadygov and D. R. Yarkony, J. Chem. Phys. **110**, 3639 (1999).